AD-A127 895 VARIATION OF EQUATORIAL F-REGION IRREGULARITY PARAMETERS AS A FUNCTION OF.. (U) TURKU UNIV (FINLAND) INSTITUTUM GEOGRAPHICUM E MACKENZIE ET AL. NOV 82 1/1

UNCLASSIFIED SCIENTIFIC-2 AFGL-TR-82-0369 F/G 4/2 NL

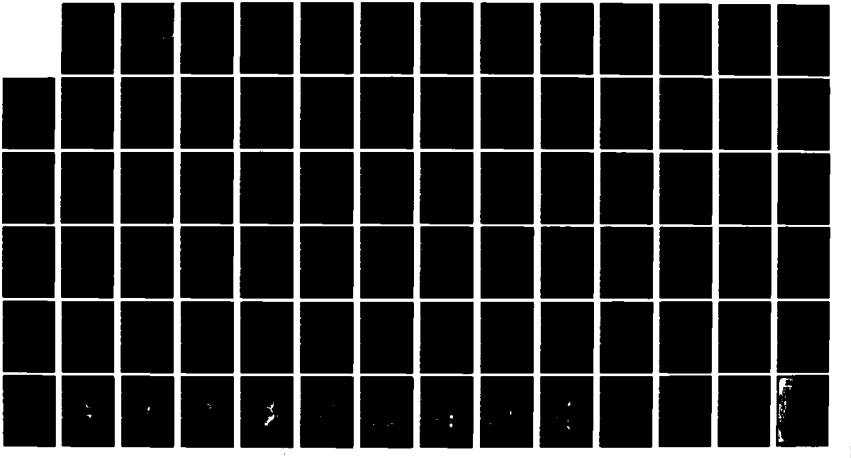

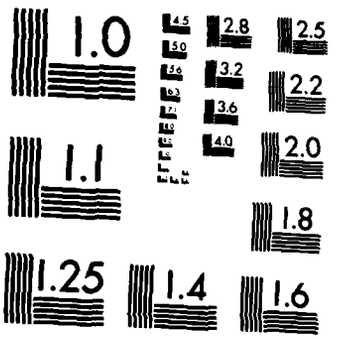

AFGL-TR-82-0369

VARIATION OF EQUATORIAL F-REGION IRREGULARITY PARAMETERS AS A FUNCTION OF SOLAR ACTIVITY

Eileen MacKenzie
Santimay Basu

The Trustees of Emmanuel College
400 The Fenway
Boston, Massachusetts 02115

Scientific Report No. 2

November 1982

This research was partially supported by the Defense Nuclear Agency, Subtask I25AAXHX, and the Space Division, Project 2029.

Approved for public release; distribution unlimited

AIR FORCE GEOPHYSICS LABORATORY
AIR FORCE SYSTEMS COMMAND
UNITED STATES AIR FORCE
HANSCOM AFB, MASSACHUSETTS 01731

MIL-STD-847A
31 January 1973

Unclassified
SECURITY CLASSIFICATION OF THIS PAGE (When Data Entered)

REPORT DOCUMENTATION PAGE	READ INSTRUCTIONS BEFORE COMPLETING FORM
1. REPORT NUMBER: AFGL-TR-82-0369	2. GOVT ACCESSION NO.: AD-A127695
	3. RECIPIENT'S CATALOG NUMBER:
4. TITLE (and Subtitle): VARIATION OF EQUATORIAL F-REGION IRREGULARITY PARAMETERS AS A FUNCTION OF SOLAR ACTIVITY	5. TYPE OF REPORT & PERIOD COVERED: Scientific Report No. 2 14 Nov 81 - 14 Nov 82
	6. PERFORMING ORG. REPORT NUMBER:
7. AUTHOR(s): Eileen MacKenzie Santimay Basu	8. CONTRACT OR GRANT NUMBER(s): F19628-81-K-0011
9. PERFORMING ORGANIZATION NAME AND ADDRESS: The Trustees of Emmanuel College 400 The Fenway Boston MA 02115	10. PROGRAM ELEMENT, PROJECT, TASK AREA & WORK UNIT NUMBERS: 62101F 4643AAAB
11. CONTROLLING OFFICE NAME AND ADDRESS: Air Force Geophysics Laboratory Hanscom AFB MA 01731 Contract Monitor: Herbert E. Whitney/PHY	12. REPORT DATE: November 1982 13. NUMBER OF PAGES: 79
14. MONITORING AGENCY NAME & ADDRESS (if different from Controlling Office)	15. SECURITY CLASS. (of this report): Unclassified 15a. DECLASSIFICATION DOWNGRADING SCHEDULE

16. DISTRIBUTION STATEMENT (of this Report)

A - Approved for public release; distribution unlimited.

17. DISTRIBUTION STATEMENT (of the abstract entered in Block 20, if different from Report)

Tech, other

18. SUPPLEMENTARY NOTES

This research was partially supported by the Defense Nuclear Agency, Subtask I25AAXHX, and the Space Division, Project 2029.

19. KEY WORDS (Continue on reverse side if necessary and identify by block number)

Spread-F	Airglow
Ionograms	In-situ density measurements
50 MHz radar backscatter	Spaced-receiver
Scintillations	Solar activity

20. ABSTRACT (Continue on reverse side if necessary and identify by block number)

The Air Force Geophysics Laboratory in collaboration with the Geophysical Institute of Peru and the University of Texas at Dallas performed co-ordinated measurements of nighttime F-region irregularities near the magnetic equator during 1975-1979. A variety of techniques, such as ionospheric soundings, scintillation, airglow, VHF radar backscatter and satellite

DD FORM 1 JAN 73 1473 EDITION OF 1 NOV 65 IS OBSOLETE

Unclassified
SECURITY CLASSIFICATION OF THIS PAGE (When Data Entered)

Unclassified
SECURITY CLASSIFICATION OF THIS PAGE(When Data Entered)

in-situ density probes, were employed to study the F-region irregularities over a wide scale-length range from tens of kilometers to a few meters. The dynamics of the irregularity structures were explored by the Airborne Ionospheric Observatory of the Air Force Geophysics Laboratory as well as by the spaced receiver scintillation measurements performed on the ground. This report compiles some of these measurements with a view to studying the variation of the irregularity characteristics with changes in solar activity that occurred during the campaign periods in the years 1975-1979.

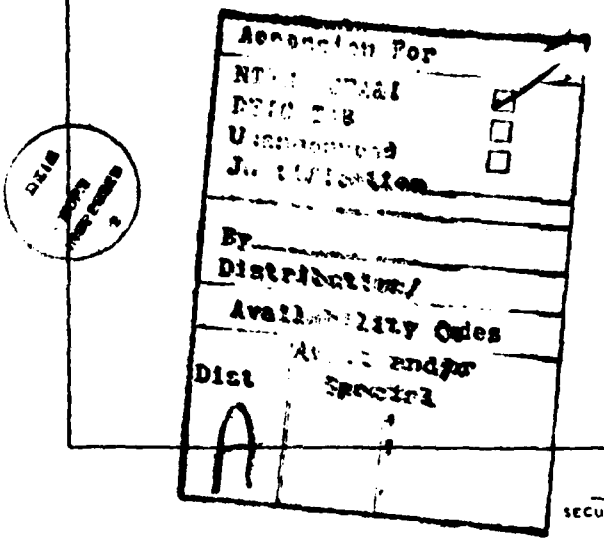

Unclassified
SECURITY CLASSIFICATION OF THIS PAGE(When Data Entered)

VARIATION OF EQUATORIAL F-REGION IRREGULARITY PARAMETERS AS A FUNCTION OF SOLAR ACTIVITY

Eileen MacKenzie and Santimay Basu
Emmanuel College
Physics Research Division
400 The Fenway
Boston MA 02115

ABSTRACT

The Air Force Geophysics Laboratory in collaboration with the Geophysical Institute of Peru and the University of Texas at Dallas performed co-ordinated measurements of nighttime F-region irregularities near the magnetic equator during 1975-1979. A variety of techniques, such as ionospheric soundings, scintillation, airglow, VHF radar backscatter and satellite in-situ density probes, were employed to study the F-region irregularities over a wide scale-length range from tens of kilometers to a few meters. The dynamics of the irregularity structures were explored by the Airborne Ionospheric Observatory of the Air Force Geophysics Laboratory as well as by the spaced receiver scintillation measurements performed on the ground. This report compiles some of these measurements with a view to studying the variation of the irregularity characteristics with changes in solar activity that occurred during the campaign periods in the years 1975-1979.

1. INTRODUCTION

The Air Force Geophysics Laboratory in collaboration with the Geophysical Institute of Peru and the University of Texas at Dallas developed a joint program of study during 1975-1979 to evaluate the effects of nighttime equatorial ionospheric irregularities on satellite communications and VHF radar backscatter and to determine the mechanisms responsible for the generation of irregularities in the equatorial ionosphere. With these objectives in view, coordinated observations of equatorial F-region irregularities were performed by various techniques (ionosonde, VHF/UHF scintillations, spaced receiver drifts, airglow, satellite in-situ and radar backscatter) near the magnetic equator in the Peruvian sector during selected campaign periods in the years 1975-1979. Since this period covered widely varying levels of solar activity, these results are utilized to investigate the characteristic variation of the irregularity parameters with solar activity.

Until recently, the spread-F signature on ionograms and scintillation data have been the primary methods used to study the nighttime F-region irregularities of electron density at equatorial latitudes. Now additional techniques, such as satellite in-situ, radar backscatter and spaced receiver scintillation measurements are available to supplement these methods by providing extended coverage of irregularity scale-lengths and considering the

irregularity motion (Basu and Aarons, 1977, AFGL-TR-77-0264, and references therein). The ionogram analysis obtained during the joint study period (1975-1979) is presented in Section 2, while corresponding scintillation analysis is shown in Section 3. The results of irregularity drift measurements are discussed in Section 4, the spatial variations of electron density by satellite in-situ probes in Section 5, the 50 MHz radar backscatter observations in Section 6, and the airglow and ionosonde measurements on the aircraft in Section 7. The stations at Ancon and Huancayo and the coordinates (Ancon L9 and Huancayo MS) pertaining to these measurements are illustrated in Figure 1. The position of LES-9 changed as a function of time (1977-1979) while Marisat remained fixed throughout the period 1976-1979. During 1975, no coordinated scintillation and radar measurements were performed; only radar backscatter and ionogram analysis for this period are included in the report. The ionosonde data were obtained at Huancayo (H) and scintillation measurements were performed from both Ancon (A) and Huancayo (H).

2. IONOGRAM ANALYSIS – VIRTUAL HEIGHT AND SPREAD-F

Early observations of equatorial spread-F at Huancayo (Booker and Wells, 1938) indicated that the onset of spread-F is preceded by a rapid increase of F-layer height after sunset. In view of the possibility of using this parameter to predict the onset of natural spread-F or to determine the ionospheric conditions suitable for triggering artificial spread-F, the post-sunset increase in F-layer height has recently engaged the attention of workers in this field.

In the following, this problem is studied by the use of ionogram data obtained at Huancayo, Peru (12.1°S, 75.3°W) during the campaign periods. The data base consists of limited nights (<10) during each of 5 periods over 5 years (1975-1979) as indicated in Table 1. The monthly mean sunspot number corresponding to each of the campaign periods is also shown in the table.

Table 1

Dates	No. of Nights	Sunspot No.
Nov. - Dec. 1975	10	15
Oct. 1976	7	21
Mar. 1977	9	8
Mar. 1978	7	73
Mar. 1979	4	137

From the ionograms, the virtual heights corresponding to the

base of the F-region (h_{min}) was determined and the spread-F was categorized into two types, range and frequency spread (Rastogi, 1980a). The spread of the ionogram trace in the presence of a curvature of the trace signifying underlying F-region ionization is grouped under frequency spread and that obtained in the absence of curvature is grouped under range spread. In addition, the spread signature confined only to the base of the F-layer, is grouped under the term bottomside range spread. In order to provide an idea of the evolution of the two types of spread F, the results of the ionogram analysis for the selected days in the campaign periods during 1977-1979 are shown in Table 2. The symbol r denotes bottomside spread F, R denotes total range spread F, F denotes frequency spread F and a blank denotes no spread. It may be noted that the bottomside spread-F first appears and may persist for 15-60 minutes before the total range spread occurs. Near midnight, mixed or a combination of range and frequency spread is obtained and finally pure frequency spread results which often persists till sunrise. Thus, the bottomside spread-F marks the onset and frequency spread the end of the activity.

We now investigate the variation of h_{min} for each of the 5 campaign periods during the time interval $\sim$1700-2100 local time. This is the time period of post-sunset increase of the F-layer altitude prior to the possible onset of spread-F. On certain days, the spread F occurrence curtails

readings in the 20-21 local time (LT) segment. The variation of h_{min} with LT is shown in Figures 2a-e in a format similar to that used by Tsunoda and Rino (1982) to show the diurnal variation of h'F at Kwajalein in August 1981. In Figures 2a-e, a dot (•) signifies h_{min}, a bar (|) the presence of bottomside spread-F, and an asterisk (*) the presence of total range spread F. Since the data were obtained from routine ionospheric soundings, the time resolution of the plots is 15 minutes. The plots for successive days are displaced upwards, the datum level of 200 km for each plot being indicated by an arrow. It may be noted that the F-layer rises after sunset, attains a maximum altitude, and then commences to fall. During the sunspot minimum period (1975-1977) the time variation of h_{min} shows a broad featureless maximum whereas in the sunspot maximum period (1978-1979) a pronounced maximum is observed. The onset of the bottomside or total range spread (denoted by | or *) takes place over either the broad-maximum or the descending phase of h_{min}. On many occasions, two maxima of h_{min} are observed, a small primary maximum being followed by a more pronounced secondary maximum. In such cases, the onset of spread-F usually takes place following the primary maximum. The secondary maximum is possibly a signature of the height modulation of the base of the F-layer caused by the development of a bubble (Scannapieco and Ossakow, 1976).

Table 3 shows the salient features of the Figures 2a-e. It lists the maximum rate of rise of hmin in meters per

second observed during any 15 min interval prior to the onset of spread-F, the time of this maximum rate of rise and the time of spread-F onset. The range and the average values of each column are listed at the bottom for each of the campaign periods. It should be emphasized that the time resolution of the data is 15 minutes and, therefore, the upward drift speed, listed in Table 3, represents only the lower bound of this parameter. A notation is shown next to the nights on which plumes were seen. These will be discussed in Section 6.

Each of the campaign periods was grouped together and Table 4 lists the range of values of h_{min} and the average of the maximum upward velocity of the base of the F-layer observed prior to the onset of spread-F. It may be noted that h_{min} increases with increasing sunspot number and an increase of the altitude by as much as 150 km occurred between 1975-1979. Thus the threshold altitude at which the spread-F occurs depends on the level of solar activity. The upward velocity of the F-layer does show some variation with season as well as the solar activity and, therefore, the increase as a function of solar activity is best studied from the last three rows in Table 4 representing the same month of March in 1977, 1978, and 1979. A consistent increase of the upward drift speed with an increase of sunspot number may be noted.

In summary, the F-layer rises in the post-sunset hours, the rise being more pronounced during the sunspot

Table 4

Campaign	h_{min} Prior to Spread-F (km)	Average Rate of Increase of h_{min} (m/sec)	Sunspot No.
Nov-Dec 1975	230 - 310	13	15
Oct 1976	255 - 310	26	21
Mar 1977	270 - 330	19	8
Mar 1978	350 - 400	33	73
Mar 1979	370 - 400	42	137

maximum period. The onset of spread-F occurs either during the period when the base of the F-layer attains a broad maximum or during the descending phase of the F-layer. The former alternative is a characteristic of the sunspot minimum period and the latter is a feature of the sunspot maximum period. The different types of spread-F usually follows a time sequence. The nighttime spread-F activity starts with the appearance of the bottomside spread-F, which is followed by a prolonged period of range spread activity, then a mixture of frequency and range spread, and finally the onset of pure frequency spread marks the end of the activity on a given night. Both types of spread-F activity are observed during the sunspot minimum as well as the maximum period. The threshold altitude at which the spread-F onset takes place varies from 300 km to 400 km depending on whether the solar activity is minimum or maximum. The upward velocity of the F-layer that gives rise to the post-sunset rise of the F-layer

increases with solar activity and is observed to change by a factor of 2 between 1977 and 1979.

3. SCINTILLATIONS

The sudden onset of spread-F in the equatorial region during the post-sunset hours, discussed in the previous section, is accompanied by an equally abrupt development of scintillations in the VHF-UHF range of frequencies. Scintillations are observed in a series of distinct patches, each patch lasting for a period of about an hour. Daily plots of scintillations in October 1976, March 1977 (Whitney et al., 1977), and March 1978 (Whitney, 1979) campaign periods illustrate these features. Figures 3a-3e complete this data base by providing the temporal variation of scintillation magnitudes observed on the 249 MHz transmissions from the near synchronous satellite LES-9 at Ancon, Peru during the March 1979 campaign. The ordinate shows the peak to peak signal excursions in dB (Whitney, 1969) and the abscissa the universal time (UT $\approx$ LT + 5 hours). It may be noted that scintillation magnitudes at 249 MHz exceed 25 dB and are confined within distinct temporal structures each lasting for a period of about an hour. The time variation of scintillations shown in Figures 3b-3e may be compared with the sequence of spread-F occurrence shown in Table 2. For example, the delayed onset of range and frequency type spread-F on March 22-23, 1979 observed in Huancayo ionograms correlate very well with the delayed onset of scintillations on this night as shown in Figure 3e.

The results of scintillation measurements performed at

Ancon with the 249 MHz transmissions from the LES-9 satellite during the three March campaigns in 1977-1979 may be used to study the variation of scintillations with solar activity. Due to the movement of the satellite, the 350 km sub-ionospheric position of LES-9 (i.e., the intersection of the propagation path with the 350 km ionospheric height) varied in each year. Figure 1 shows the locus of the 350-km sub-ionospheric position of LES-9 for each year and is indicated by A(L-9). The ground station at Ancon (A) and Huancayo (H) as well as the sub-ionospheric position of the Marisat satellite as viewed from Huancayo are shown in the diagram. Figures 4a-4c show the percentage occurrence of 249 MHz scintillations exceeding 10 dB as a function of UT in each of the campaign periods. The abrupt onset of scintillations at about 00 UT corresponding approximately to 1900 LT and the maximum percentage occurrence of 249 MHz scintillations exceeding 60% is noted. The persistence of scintillations in the post-midnight period during 1978 and 1979 is found to be a major feature of high solar activity. In view of the short duration of each campaign, the continuous 257 MHz scintillation measurements made at Huancayo with the Marisat satellite is shown in Figure 5 for the month of March during 1977-1979. The features mentioned earlier are reproduced in this diagram and progressively higher scintillation occurrence in the post-midnight period with increasing solar activity between 1977-1979 is noted. This persistence of

the post-midnight scintillations is probably due to the enhanced ionization density available in this time interval during the solar maximum period. It may be mentioned that scintillation magnitudes are controlled primarily by the integrated electron density deviation (ΔN) over the irregularity layer thickness. This parameter (ΔN) is thus a product of the irregularity amplitude ($\Delta N/N$), the background electron density (N), and the irregularity layer thickness. When F-region irregularities are encountered over the equatorial region in the nighttime hours, a few percent irregularity amplitudes are always obtained. On the other hand, the background F-region density in the nighttime hours is increased by about a factor of 10 during sunspot maximum. Thus the preponderance of irregularities and high background ionization density during sunspot maximum increases greatly the scintillation magnitudes and their duration.

In contrast to the scintillation measurements with geostationary satellites discussed in this section, the SRI International performed phase and amplitude scintillation measurements with the orbiting Wideband satellite during the March, 1977 campaign period which provided a much broader spatial coverage over a short period of time. The results of these observations are very well summarized in Rino et al. (1977) and will not be repeated here.

4. IRREGULARITY DRIFT MEASUREMENTS

During each of the 3 campaign periods, spaced receiver scintillation measurements were conducted at Ancon, Peru by recording scintillations on two independent receiving systems with their antennas located on an east-west baseline of 366 m. Near the magnetic equator, the F-region irregularities are highly elongated in the magnetic north-south direction and the only observable velocity is in the east-west direction (Briggs and Golley, 1968). The measured velocity is called the apparent eastward velocity. Cross-correlation analysis was performed on the two digitized data channels each of 3 minutes duration and the time delay yielding the maximum correlation was combined with the known distance of separation to obtain the east-west drift speed. Figures 6a (March 1977), 6b (March 1978), and 6c (March 1979) show 15-min averages of this data plotted against time. The diagrams indicate that the equatorial F-region irregularities drift towards the east in the nighttime hours and the drift magnitudes vary by a factor of about 3-4 during this period. The variation in the drift speed affects greatly the temporal structure of equatorial scintillations. The most noticeable feature of the Figures 6a-6c is the extension of a high drift velocity into the post-local-midnight time period (local time = UT - 5 hours) seen in the March 1978 data (Figure 6b). To a lesser extent, this is also seen in the March 1979 plot (Figure 6c), but a paucity of data in

this time period precludes easy identification. It may be noted that the east-west drift is a result of ExB forces, E being the vertical electric field and B the magnetic field intensity. Thus from a knowledge of the eastward drift speed, the vertical electric field may be estimated.

5. SATELLITE IN-SITU DENSITY MEASUREMENTS

The in-situ measurements of electron concentration and its fluctuations by the Atmosphere Explorer-E (AE-E) satellite over the equatorial F-region provide information on the spatial structure of the irregularities that are probed by various ground-based techniques. Recently, in-depth studies of the spectral characteristics of the equatorial F-region irregularities have been performed and related to the temporal structure of scintillations (Basu and Whitney, 1982; Basu et al., 1982). In this section, we shall concentrate on the in-situ data over the Peruvian sector during the campaign periods when a variety of ground based measurements were available. It is, however, difficult to obtain co-ordinated transits of a satellite during the short campaign periods. As a result, this data base is more limited than others presented here (ionograms, scintillation and radar backscatter maps) and has been used in individual case studies coordinated with the other measurements. One such study is shown in Basu et al. (1980). Over the 5 campaign periods mentioned in Section 2, only 6 cases are available for such a coordinated study. All but one of these cases present the signature of "bubbles" (McClure et al., 1977) associated with "plumes" (Woodman and Lalloz, 1976) similar to that represented by the March 20-21, 1977 data shown in Basu et al. (1980). The sixth case is shown here for its uniqueness.

Figure 7 shows two AE-E subsatellite tracks on

March 30, 1977 between 0000-0215 UT, along with the Jicamarca ground station where 50 MHz radar backscatter observations are performed. Figures 8 and 9 illustrate the ion concentration fluctuations between 17-20 MLT over the longitude interval 100°W to 70°W obtained by the ion drift meter on board AE-E. Although the satellite samples at an altitude of 275 km, the relative ion concentration fluctuations correspond to those at higher altitudes over the magnetic equator. The entire magnetic flux tube takes part in the instability process (Anderson and Haerendel, 1979) and therefore the relative ion concentration fluctuations can be mapped along the field lines, at least at large scale-lengths. In view of the charge neutrality at F-region heights, the fluctuations of ion concentration represent the electron concentration fluctuations. The product of the magnitude of electron concentration fluctuations at the mapped location and the local electron concentration yield the electron density deviation which is of interest in the modelling of scintillations.

The AE-E transit at 0031-0040 UT (Figure 8) indicates large scale wave type fluctuations in ion concentration. The next AE-E transit shows that the large scale fluctuations are replaced by discrete spatial regions having large short-scale fluctuations of electron density. It will be shown in the next section that the 50 MHz radar at Jicamarca detected 3-m scale irregularities at this time. The two

successive AE-E transits provide a unique display of the sequence of irregularity generation. The large-scale perturbation of the F-region, detected during the first transit, may have acted as a seeding mechanism for the subsequent plasma instability process which generated large amplitude irregularities with short scale-lengths that were detected during the second transit. It should, however, be mentioned that such a sequence of transits is extremely difficult to locate. However, if a large scale perturbation is a necessary precursor for small scale irregularities then it has considerable potential for developing predictive models of the irregularity environment.

6. RADAR BACKSCATTER

During the campaign periods, radar backscatter observations at 50 MHz were performed at the Jicamarca Observatory in close proximity to other ground based measurements discussed in the previous sections. The digital power mapping technique applied to these backscatter observations provide maps of the range and intensity of VHF backscatter as a function of time which has enhanced our knowledge of equatorial spread-F (Woodman and LaHoz, 1976). It should be noted that the 50 MHz backscatter arises from the irregularities with 3-meter scale-lengths. On the other hand, intensity scintillations in the VHF-UHF frequency band are caused by the irregularities in the scale-length range of about 100 meters to 1 km. Scintillation and radar backscatter data were first utilized by Basu et al. (1977) to explore the relationship between the meter and longer scale irregularities in the equatorial spread-F. Subsequently, measurements of F-region irregularity by radar backscatter, scintillations, ionosonde and satellite in-situ techniques were carefully co-ordinated during the campaign periods to investigate the structure of the irregularities in the different scale-length regime, their evolution and decay (Basu et al., 1978; Aarons et al., 1980; Basu and Basu, 1981 and references therein).

In this section, we have attempted to integrate the radar backscatter observations made at Jicamarca during all

the campaigns covering the period 1976-1979 as well as those during Nov-Dec 1975 made available to us by J.P. McClure of the University of Texas at Dallas.

Figures 10a-10e illustrate one backscatter map for each year. The maps illustrate the temporal variation of range and intensity of the backscattering regions. During 1975-1977, the maximum range of the backscatter maps was limited to 700 km but it was extended to 1000 km during 1978 and 1979. The various decibel levels of relative intensity are indicated by different shades in the diagrams, the darker shades corresponding to more intense irregularities. Except for Figure 10a, all maps indicate that the 3-m irregularity structures are often extended in altitude by several hundred kilometers resembling 'plumes' (Woodman and LaHoz, 1976). Several such plume structures are observed between the sunset and midnight time period. The base of the irregularity structures are usually continuous and sometimes modulated in altitude. This altitude modulation is more marked in Figures 10d and 10e which correspond to the sunspot maximum period. In addition, the plumes have varying amounts of tilts. Since the irregularities drift towards the east in the equatorial region during the nighttime hours, a tilt of the plume towards increasing time signifies that in the spatial domain the irregularities are tilted towards the west. Comparing Figures 10c-10e, it becomes apparent that the plume structures become more vertical with increasing

solar activity. Figure 10a shows that on some nights plumes may not develop and instead the irregularities remain confined within a layer of about 50 km thickness. Figure 10a also shows that 3-m irregularities may be detected as late as 0200 LT. On some occasions, the 3-m irregularities are detected in the pre-sunrise period.

The long period modulation of the base of the plume structures so marked in some backscatter maps as in Figures 10d and 10e has been studied from the point of view of seeding mechanism of spread-F by long period gravity waves. However, these amplitude modulated bottomside backscatter structures (AMBB) are usually observed in association with the plume structures rather than as precursors of spread-F. Tsunoda and White (1980) have discussed some cases in which the bottomside backscattering regions first developed from the western walls of the height modulated F-region and finally the plumes were observed from the crests of these regions. The modulation period of the AMBB structures corresponds to about an hour which translates to spatial dimensions of about 400 km for an average irregularity drift speed of 100 m/sec in the nighttime equatorial region. The ionogram data discussed in Section 2 were examined in conjunction with the backscatter maps to determine the presence of any corresponding signature in the h_{min} data. It was found the h_{min} data usually provides a signature corresponding to the first AMBB structure in the evening but sub-

sequent heavy spread around h_{min} precludes any such comparison with the later structures. This signature is the post-sunset rise and the subsequent fall in h_{min}. On certain nights, when the different spread-F structures were separated by quiet periods lasting for a period of about an hour, the rise and fall of h_{min} associated with each of the spread-F structures could be determined. Thus the height modulation in h_{min} and the AMBB structures are spatial structures that drift with the spread-F and the plume structures. In the ionogram data or in the backscatter maps we could not determine an unequivocal signature of the long-period wave type fluctuations that may be viewed as precursors to subsequent spread-F generation. The routine 15-minute ionograms occasionally exhibited an oscillatory variation of h_{min} prior to the onset of spread-F. This variation may be studied with higher time resolution of ionosonde soundings to determine if it is possible to isolate any distinctive precursor of spread-F.

Following Aarons et al. (1980) we illustrate in Figures 11a-11c, composite contours of the percent occurrence of backscatter echoes within 6 dB of the maximum return for the period 1975-1979. We have reproduced the composite maps for Oct 1976, Mar 1977, and Mar 1978 from Aarons et al. (1980) and added the maps for Nov-Dec 1975, and Mar 1979. These maps may be studied to determine the effects of the varying solar activity between 1975-1979 on

the structure of the 3-m irregularities in equatorial spread-F. Comparing Figures 11c-11e, which belong to the same month over the period 1977-1979, it is noted that with increasing solar activity both the minimum altitude and the extent of the 3-m irregularities increase with increasing solar activity. A study of the backscatter maps on individual nights as shown in Figures 10c-10e, indicate that with increasing solar activity, the altitude modulation of the bottomside of the VHF backscatter become more pronounced, the plumes become more vertical and the extent of the plumes also increases.

7. AIRGLOW AND IONOSONDE MEASUREMENTS BY THE AIRBORNE IONOSPHERE OBSERVATORY

The instrumented aircraft of the Air Force Geophysics Laboratory was used to make all sky images of 6300 Å and 5577 Å airglow emissions in the nighttime equatorial F-region as well as perform ionosonde measurements during the campaign period. Weber et al. (1978) showed for the first time the existence of north-south magnetic field aligned regions of 6300 Å airglow depletions. They found that the dark bands of airglow depletions extend more than 1200 km in the north-south direction and 50-250 km in the east-west direction. These structures were observed to maintain their spatial integrity and drift eastwards at a speed ranging between 50-150 m/sec. Combining the simultaneous airglow and ionosonde measurements on board the aircraft, Weber et al. (1978) were able to track the motion of the ionospheric scattering regions associated with the walls of the airglow depletion structures. The two sets of measurements could be modelled by a bottomside electron density depletion as shown in Figure 12.

The magnetic field alignment of the airglow structures implied that the entire magnetic flux tube takes part in the instability process as suggested by Haerendel (1974).

8. SUMMARY

It has been shown that following the post-sunset rise of the F-region, the generation of equatorial spread-F takes place when the F-region plasma enters its descending phase. The altitude at which the onset of spread F is observed varies by as much as 200 km depending on the level of solar activity.

The post-sunset increase in F region altitude caused by the enhanced eastward electric field as well as the onset altitude of spread F are observed to be significantly higher during the solar maximum period. However, the full range of spread F phenomena encompassing saturated VHF/UHF scintillations (km-scale irregularities) and intense radar plume structures (3-m irregularities) are encountered at all levels of solar activity. The usually observed westward tilts of the plume structures are observed to undergo changes with solar activity, the plumes becoming more vertical with increased activity. The spaced receiver scintillation measurements indicate a trend of increased eastward drift speed in the post-midnight hours during sunspot maximum period signifying a persistence of enhanced vertical electric field. Thus during solar maximum period, enhancements of both the pre-reversal electric field in the post-sunset period as well as enhanced vertical electric field in the post-midnight hours are encountered.

The coordinated multi-technique measurements of

equatorial spread-F performed during the campaign periods have considerably advanced our knowledge of spread-F generation and decay. It has been established that the spread-F occurs in distinct patches with overall E-W dimensions of the order of several hundred kilometers. These patches contain sub-structures or "bubbles", with E-W dimensions of the order of few tens of kilometers. The bubbles may contain irregularities spanning a wide range of scale-lengths from tens of km to tens of cm.

These patches retain their identity and drift towards the east and give rise to the temporal variation of various observed parameters, e.g., phase and intensity of satellite signals, airglow and radar backscatter (Aarons et al., 1978; Basu et al., 1978; Weber et al., 1978).

The generation of such a wide range of irregularity scale-lengths can be explained only by invoking several instability processes in a step by step manner which utilizes the large scale primary irregularities as a seed for the generation of small scale irregularities (Haerendel, 1974; Fejer and Kelley, 1980). From an observation point of view, however, the wide range of scale sizes have been detected simultaneously. It has not been generally possible to isolate a finite amplitude large scale perturbation of the background ionosphere preceding the formation of spread-F. Neither have we been able to explain the presence of scintillation on a string of days and their absence in the following few

days. The answers to these questions will obviously help us develop predictive models for equatorial scintillations.

ACKNOWLEDGMENT

This report is based on data obtained by many dedicated scientists from different organizations. We would first like to thank the Instituto Geofisico del Peru for making it possible to conduct the joint program of study and their technical staff, A. Bushby, J. Pantoja, and J. Lanat. We thank J. Aarons, associated with the AFGL during the campaign period, for formulating the joint program of study and maintaining a constant flow of discussions on scientific results. J.P. McClure of the University of Texas at Dallas kindly placed at our disposal the backscatter results from his operation of the Jicamarca radar. H. Whitney and J.P. Mullen of AFGL were responsible for the scintillation data acquisition at the field sites. Optical, scintillation, and ionospheric sounding measurements from the AFGL Airborne Ionospheric Observatory were performed by J. Buchau and E. Weber. The Atmosphere Explorer-E satellite in-situ data were kindly provided to us by W.B. Hanson and J.P. McClure of the University of Texas at Dallas. We express our thanks to Dr. Sunanda Basu for a critical reading of the manuscript and scientific discussions.

The work was supported by AFGL Contract No. F19628-81-K-0011.

REFERENCES

Aarons, J., J. Buchau, S. Basu, and J.P. McClure (1978) The localized origin of equatorial F-region irregularity patches, J. Geophys. Res., 83, 1659.

Aarons, J., J.P. Mullen, H.E. Whitney, and E.M. MacKenzie (1980) The dynamics of equatorial irregularity patch formation, motion, and decay, J. Geophys. Res., 85, 139.

Anderson, D.N. and G. Haerendel (1979) The motion of depleted plasma regions in the equatorial ionosphere, J. Geophys. Res., 84, 4251.

Basu, S. and J. Aarons (1977) Equatorial irregularity campaigns, Part I: Correlated scintillation and radar backscatter measurements in October 1976, AFGL-TR-77-0264.

Basu, S. and S. Basu (1981) Equatorial scintillations — a review, J. Atmos. Terr. Phys., 43, 473.

Basu, S. and H.E. Whitney (1982) The temporal structure of intensity scintillations near the magnetic equator, Accepted for publication in Radio Sci.

Basu, S., J. Aarons, J.P. McClure, C. LaHoz, A. Bushby, and R.F. Woodman (1977) Preliminary comparisons of VHF radar maps of F-region irregularities with scintillations in the equatorial region, J. Atmos. Terr. Phys., 39, 1251.

Basu, S., S. Basu, J. Aarons, J.P. McClure, and M.D. Cousins (1978) On the coexistence of kilometer- and meter-scale irregularities in the nighttime equatorial F region, J. Geophys. Res., 83, 4219.

Basu, S., J.P. McClure, S. Basu, W.B. Hanson, and J. Aarons (1980) Coordinated study of equatorial scintillation and in-situ and radar observations of nighttime F-region irregularities, J. Geophys. Res., 85, 5119.

Basu, S., S. Basu, J.P. McClure, W.B. Hanson, and H.E. Whitney (1982) High resolution topside in-situ data of electron densities and VHF/GHz scintillations in the equatorial region, Accepted for publication in J. Geophys. Res.

Booker, H.G. and H.W. Wells (1938) Scattering of radio waves by the F-region of the ionosphere, Terr. Magn. Atmos. Elec., 43, 249.

Briggs, B.H. and M.G. Golley (1968) A test for dispersion in F-region drifts observed by the radio star scintillation method, J. Atmos. Terr. Phys., 30, 963.

Fejer, B.G. and M.C. Kelley (1980) Ionospheric irregularities, Rev. Geophys. Space Phys., 18, 401.

Haerendel, G. (1974) Theory of equatorial spread-F, report, Max-Planck Institut für Phys. und Astrophys., Garching, West Germany, 1974.

McClure, J.P., W.B. Hanson, and J.H. Hoffman (1977) Plasma bubbles and irregularities in the equatorial ionosphere, J. Geophys. Res., 82, 2650.

Rastogi, R.G. (1980) Seasonal and solar cycle variation of equatorial spread-F in the American zone, J. Atmos. Terr. Phys., 42, 593.

Rino, C.L., E.J. Fremouw, R.C. Livingston, M.D. Cousins, and B.C. Fair (1977) Wideband satellite observations, SRI International, Menlo Park, CA, Final Report, DNA001-75-C-0111.

Scannapieco, A.J. and S.L. Ossakow (1976) Nonlinear equatorial spread F, Geophys. Res. Lett., 3, 451.

Tsunoda, R.T. and B.R. White (1980) On the generation and growth of equatorial backscatter plumes — 1. Wave structure in the bottomside F layer, J. Geophys. Res., 86, 3610.

Tsunoda, R.T. and C.L. Rino (1982) A comparative analysis of equatorial spread-F and VHF scintillation, SRI International Report 1, February 1982.

Weber, E.J., J. Buchau, R.H. Eather, and S.B. Mende (1978) North-south aligned equatorial airglow depletions, J. Geophys. Res., 83, 712.

Whitney, H.E. (1979) Report on the Peru scintillation tests – March 1978, AFGL-TR-79-0030.

Whitney, H.E., J. Aarons, and C. Malik (1969) A proposed index for measuring ionospheric scintillations, Planet. Space Sci., 17, 1069.

Whitney, H.E., J. Buchau, A.L. Johnson, J.P. Mullen, and E.J. Weber (1977) Report on the Peru scintillation tests – October 1976 and March 1977, AFGL-TR-77-0282. ADA061089

Woodman, R.F. and C. LaHoz (1976) Radar observations of F-region equatorial irregularities, J. Geophys. Res., 81, 5447.

TABLE 2

March 1977

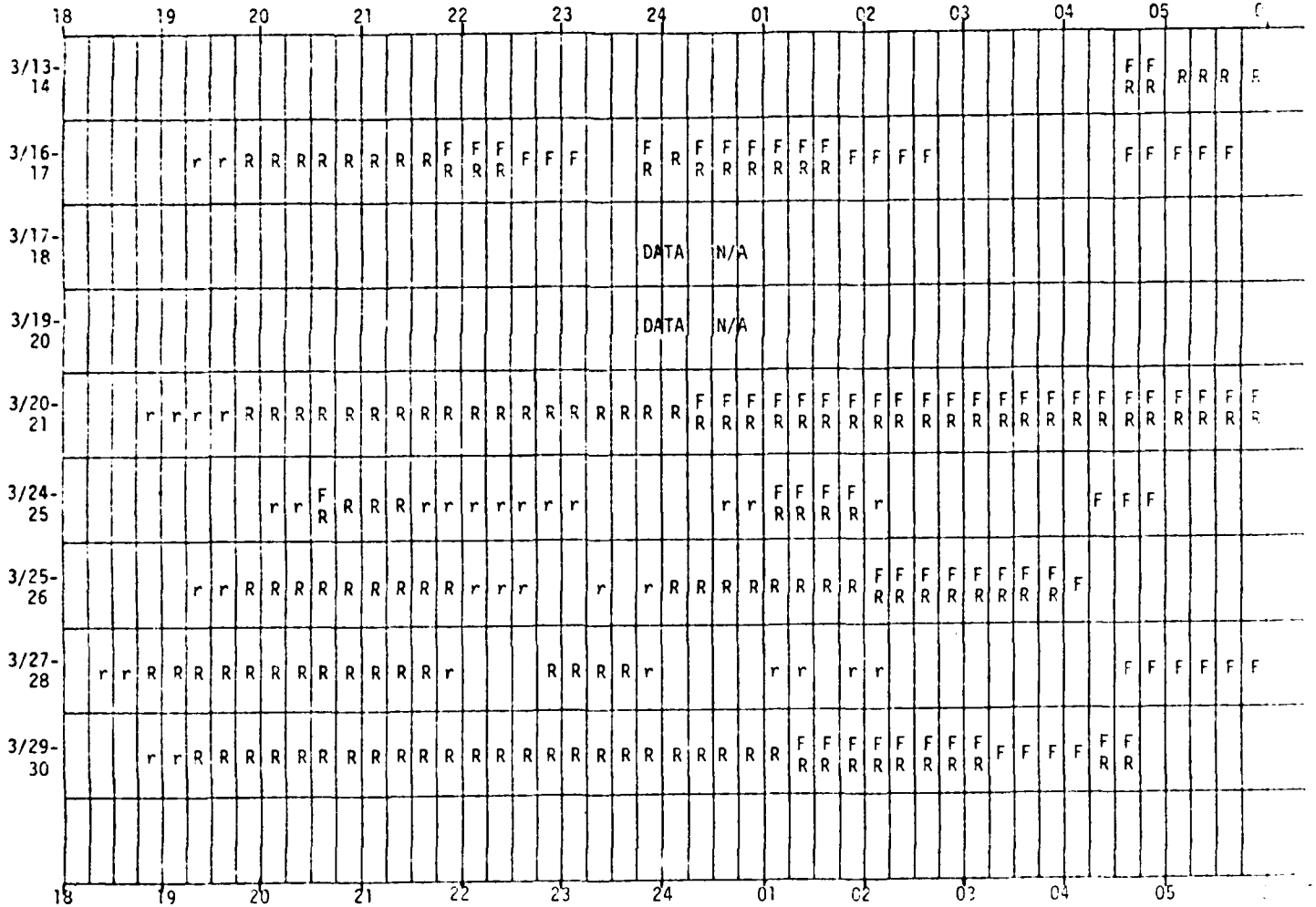

TABLE 2 (continued)

March 1978

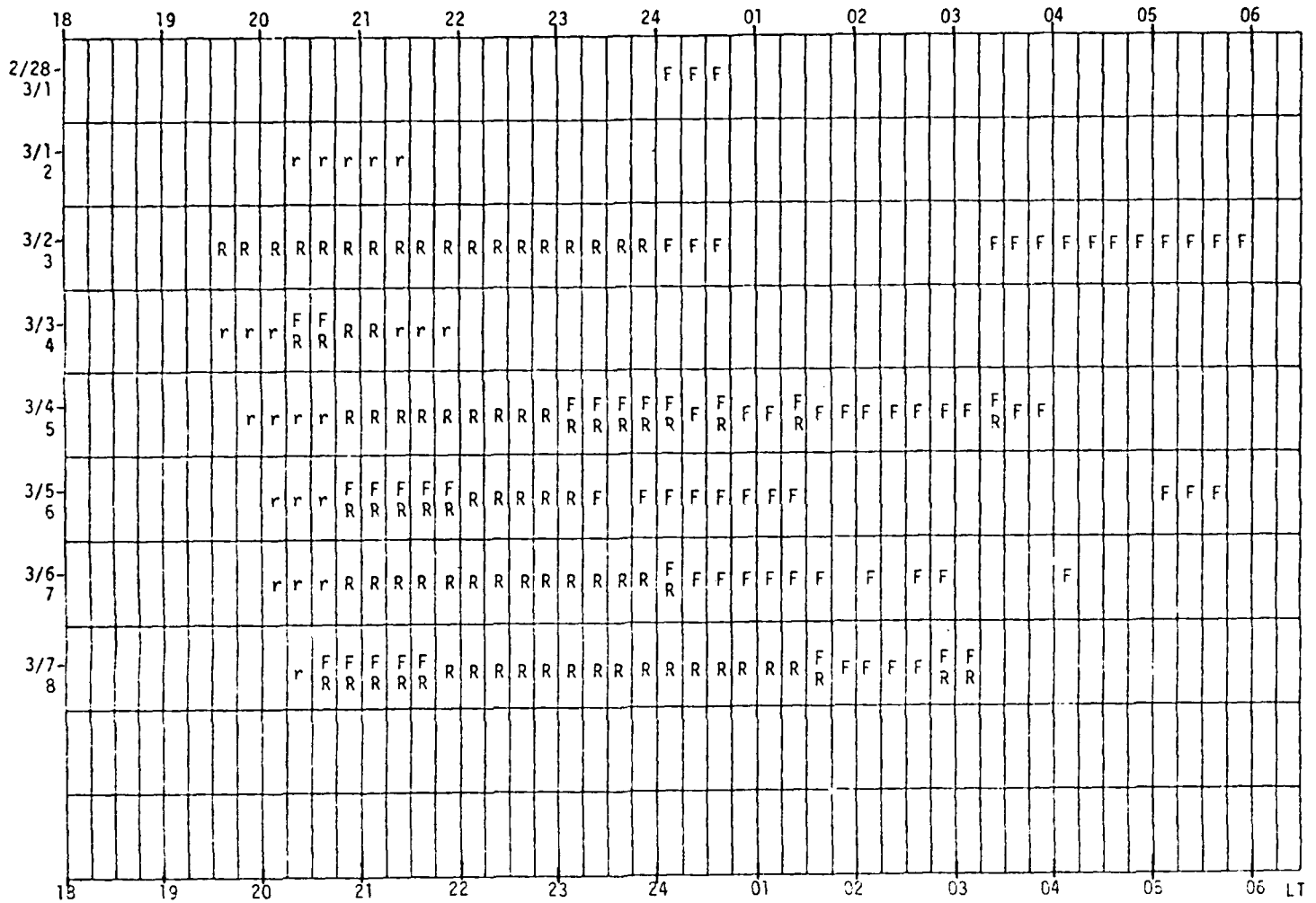

TABLE 2 (continued)

March 1979

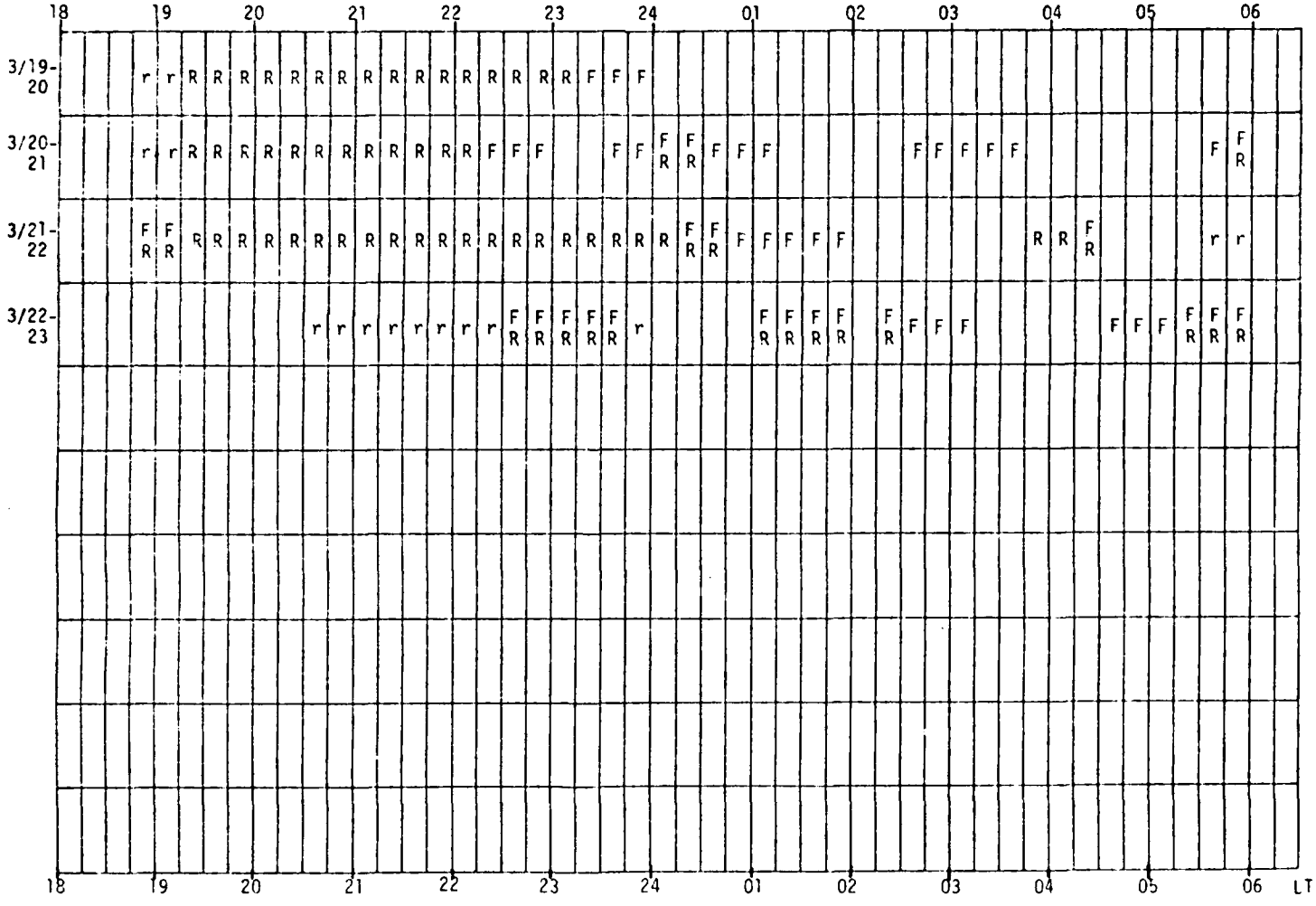

TABLE 3

Nov. - Dec. 1975

		Max Rate of Rise of h_{min} (m/sec)	Time of Max Rate of Rise of h_{min} (LT)	Onset of Time of Spread-F (LT)
11/20-21	P	17	1915-1930	1930
11/26-27	P	11	1830-1845	1900
11/27-28		17	1800-1815	1915
11/28-29		11	1800-1815	1830
12/1-2	P	17	1845-1900	1915
12/4-5		6	1800-1815	1830
12/5-6	P	11	1945-2000	2015
12/9-10	P	17	2015-2030	2100
12/10-11		11	1900-1915	1945
12/11-12	P	11	1830-1845	1915
Range:		6 - 17	1800-2000	1830-2100
Average:		13	∿1900	1915

Maximum rate of rise of h_{min} (m/sec) in any 15 min interval before onset of spread-F, time of this rise and time of onset of spread-F. A P is shown next to the dates on which plumes were seen at some time during the night.

TABLE 3 (continued)

Oct. 1976

		Max Rate of Rise of h_{min} (m/sec)	Time of Max Rate of Rise of h_{min} (LT)	Onset of Time of Spread-F (LT)
10/16-17	P	22	1830-1845	1915
10/18-19	P	56	1815-1830	1900
10/19-20	P	22	1830-1845	1915
10/20-21		17	1915-1930	———
10/21-22		28	1845-1900	1945
10/24-25	P	6	1800-1815	1900
10/29-30	P	28	1830-1845	1915
Range:		6 - 56	1800-1915	1900-1945
Average:		26	1830	1915

Maximum rate of rise of h_{min} (m/sec) in any 15 min interval before onset of spread-F, time of this rise and time of onset of spread-F. A P is shown next to the dates on which plumes were seen at some time during the night.

TABLE 3 (continued)

March 1977

		Max Rate of Rise of h_{min} (m/sec)	Time of Max Rate of Rise of h_{min} (LT)	Onset of Time of Spread-F (LT)
3/13-14		16	1845-1900	None
3/16-17		11	1845-1900	1915
3/17-18	P	11	1915-1930	1945
3/19-20	P	22	1845-1900	1915
3/20-21	P	33	1830-1845	1900
3/24-25		—	———	2015
3/25-26		28	1830-1845	1930
3/27-28	P	17	1815-1830	1845
3/29-30	P	11	1745-1800	1845
Range:		11 - 33	1745-1845	1845-2015
Average:		19	1830	1900

Maximum rate of rise of h_{min} (m/sec) in any 15 min interval before onset of spread-F, time of this rise and time of onset of spread-F. A P is shown next to the dates on which plumes were seen at some time during the night.

TABLE 3 (continued)

March 1978

		Max Rate of Rise of h_{min} (m/sec)	Time of Max Rate of Rise of h_{min} (LT)	Onset of Time of Spread-F (LT)
3/1-2		33	1845-1900	2015
3/2-3	P	44	1845-1900	1915
3/3-4		33	1845-1900	2000
3/4-5	P	33	1915-1930	1945
3/5-6		28	1915-1930	2000
3/6-7	P	28	1915-1930	2000
3/7-8		33	1945-2000	2015
Range:		28 - 44	1845-1945	1915-2015
Average:		33	1900	2000

Maximum rate of rise of h_{min} (m/sec) in any 15 min interval before onset of spread-F, time of this rise and time of onset of spread-F. A P is shown next to the dates on which plumes were seen at some time during the night.

TABLE 3 (continued)

March 1979

		Max Rate of Rise of h_{min} (m/sec)	Time of Max Rate of Rise of h_{min} (LT)	Onset of Time of Spread-F (LT)
3/19-20	P	44	1830-1845	1900
3/20-21	P	44	1830-1845	1900
3/21-22	P	50	1830-1845	1900
3/22-23		28	1830-1845	(much later)
Range:		28 - 50	1830-1845	1900
Average:		42	1830	1900

Maximum rate of rise of h_{min} (m/sec) in any 15 min interval before onset of spread-F, time of this rise and time of onset of spread-F. A P is shown next to the dates on which plumes were seen at some time during the night.

FIGURE LEGENDS

Figure 1. Geometry of ionosonde, spaced receiver and scintillation measurements. The Ancon (A) and Huancayo (H) ground stations are marked as are the 350-km subionospheric intersections of the LES-9 (observed from Ancon) and Marisat (observed from Huancayo) satellites.

Figure 2. The daily variation of the height of the base of the F-region (h_{min}) with local time for the 5 campaign periods during the time interval 1700-2100 LT.

a) Nov - Dec 1975

b) Oct 1976

c) Mar 1977

d) Mar 1978

e) Mar 1979

In these figures, a dot (•) signifies h_{min}, a bar (|) bottomside spread-F and an asterisk (*) total range spread-F.

Figure 3. Temporal variation of 249 MHz scintillation index, SI(dB), recorded at Ancon on the LES-9 propagation path during the March 1979 campaign.

a) March 19

b) March 20

c) March 21

d) March 22

e) March 23

Figure 4. Percentage occurrence of 249 MHz LES-9 scintillation observed at Ancon exceeding 10 dB as a function of UT for the following campaign periods:

a) March 1977

b) March 1978

c) March 1979

Figure 5. Percentage occurrence of 257 MHz Marisat scintillation observed at Huancayo exceeding 10 dB as a function of UT for March 1977, March 1978, and March 1979.

Figure 6. Average eastward drift velocity of irregularities obtained by cross-correlation analysis of spaced receiver data from Ancon taken in

a) March 1977

b) March 1978

c) March 1979

Figure 7. AE-E subsatellite tracks on March 30, 1977 with 2 tracks between 0000-0215 UT shown on map of Peruvian longitude sector. Jicamarca (J) ground station is also shown.

Figure 8. Ion concentration data obtained by the ion-drift meter on board the Atmosphere Explorer-E satellite during orbit #7192 on 30 Mar 1977 in the Peruvian sector showing large scale wave type fluctuations in ion concentration. UT, MLT, Dip Lat and Long are marked.

Figure 9. Ion concentration data obtained by the ion-drift meter on board the Atmosphere Explorer-E satellite during orbit #7193 on 30 Mar 1977 in the Peruvian sector showing discrete spatial regions with large short-scale fluctuations of electron density. UT, MLT, Dip Lat and Long are marked.

Figure 10. Radar backscatter observations at 50 MHz illustrating the temporal variation of range and intensity of the backscattering regions. A sample map is shown for each of the 5 campaign periods.

a) 27-28 November 1975

b) 19-20 October 1976

c) 29-30 March 1977

d) 4-5 March 1978

e) 21 March 1979

Figure 11. Composite contours of the percent occurrence of backscatter echoes within 6 dB of the maximum received power.

a) Nov - Dec 1975

b) Oct 1976 (from Aarons et al., 1980)

c) March 1977 (from Aarons et al., 1980)

d) March 1978 (from Aarons et al., 1980)

e) March 1979

Figure 12. Model of electron density depletion based on ionosonde and airglow observations made by Weber et al. (1978).

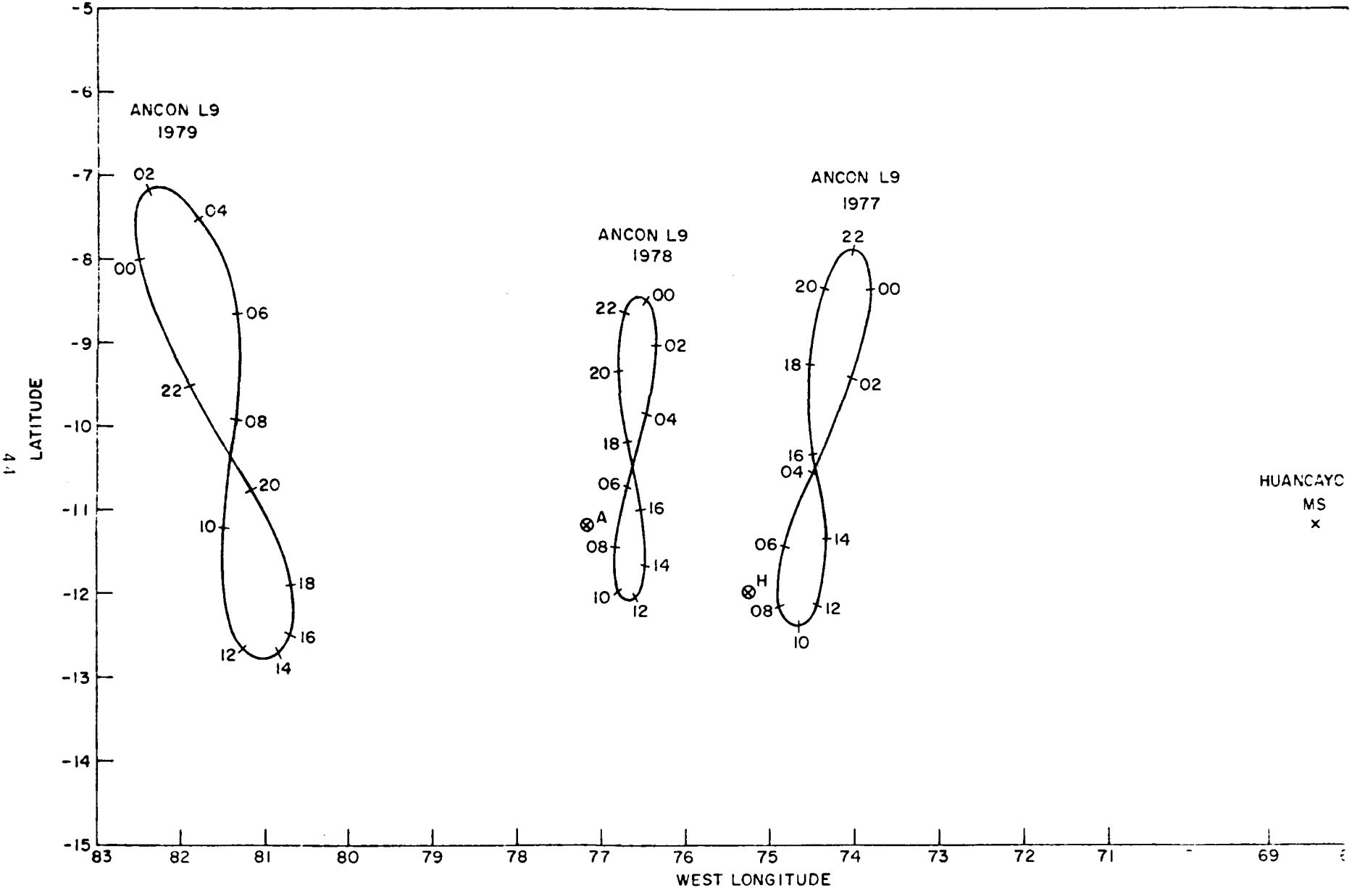
ANCON L9
1979
ANCON L9
1978
ANCON L9
1977
HUANCAYO
MS
A
H
LATITUDE
WEST LONGITUDE
-5
-6
-7
-8
-9
-10
-11
-12
-13
-14
-15
83
82
81
80
79
78
77
76
75
74
73
72
71
69
00
02
04
06
08
10
12
14
16
18
20
22

Figure 1

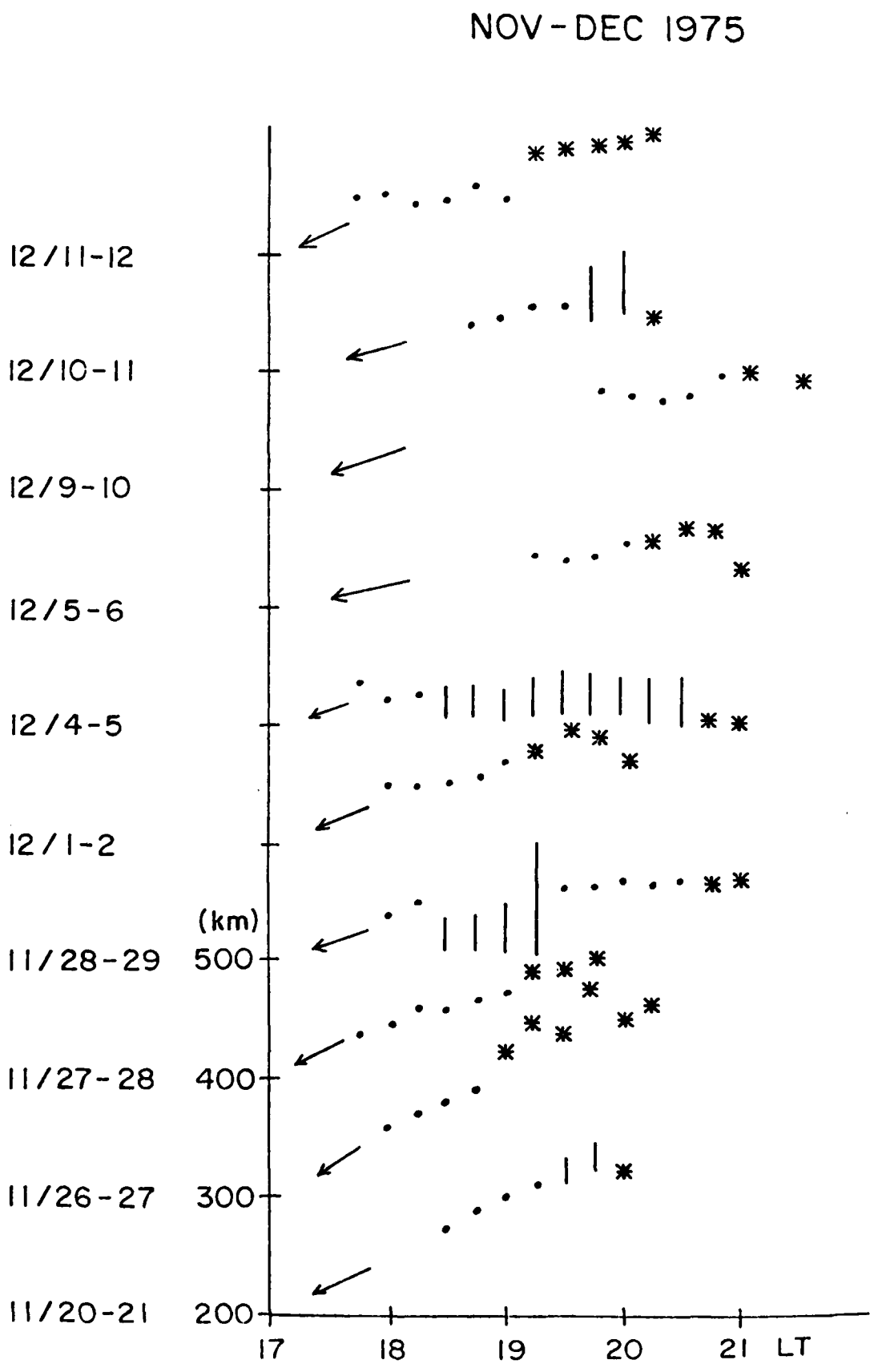
NOV-DEC 1975
12/11-12
12/10-11
12/9-10
12/5-6
12/4-5
12/1-2
11/28-29
11/27-28
11/26-27
11/20-21
(km)
500
400
300
200
17
18
19
20
21
LT

Figure 2a

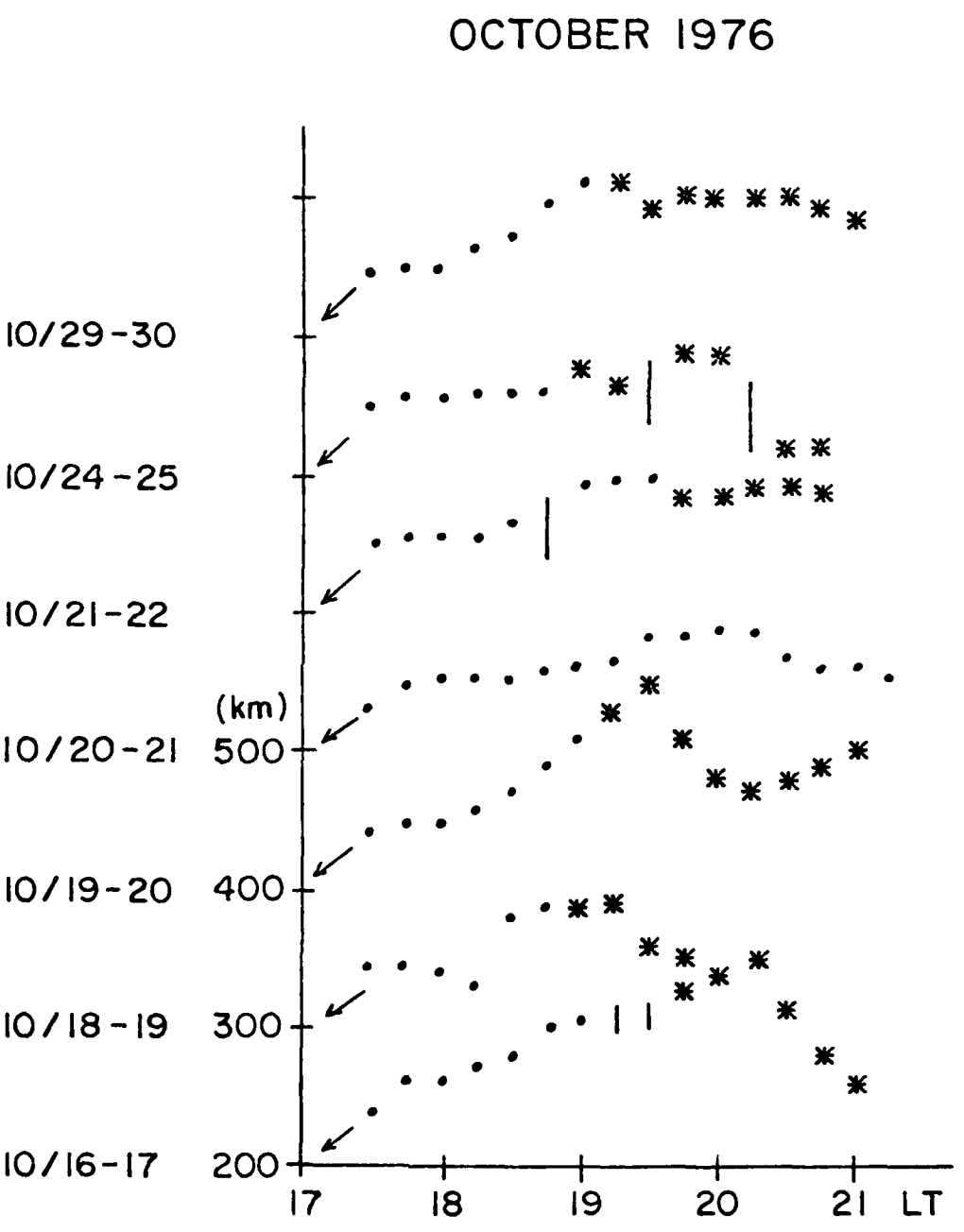
OCTOBER 1976
10/29-30
10/24-25
10/21-22
10/20-21
10/19-20
10/18-19
10/16-17
(km)
500
400
300
200
17
18
19
20
21
LT

Figure 2b

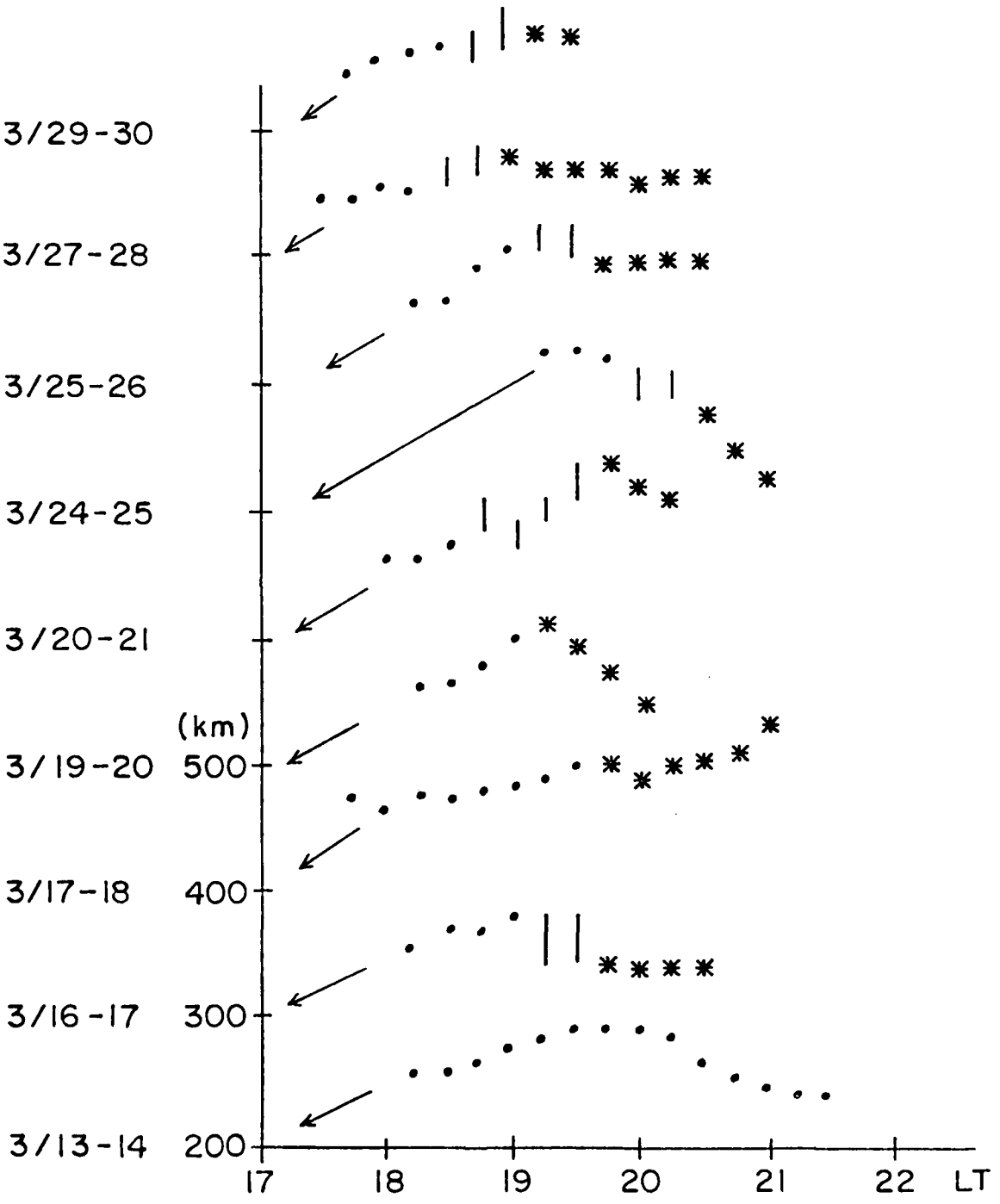
MARCH 1977
3/29-30
3/27-28
3/25-26
3/24-25
3/20-21
3/19-20
3/17-18
3/16-17
3/13-14
(km)
500
400
300
200
17
18
19
20
21
22
LT

Figure 2c

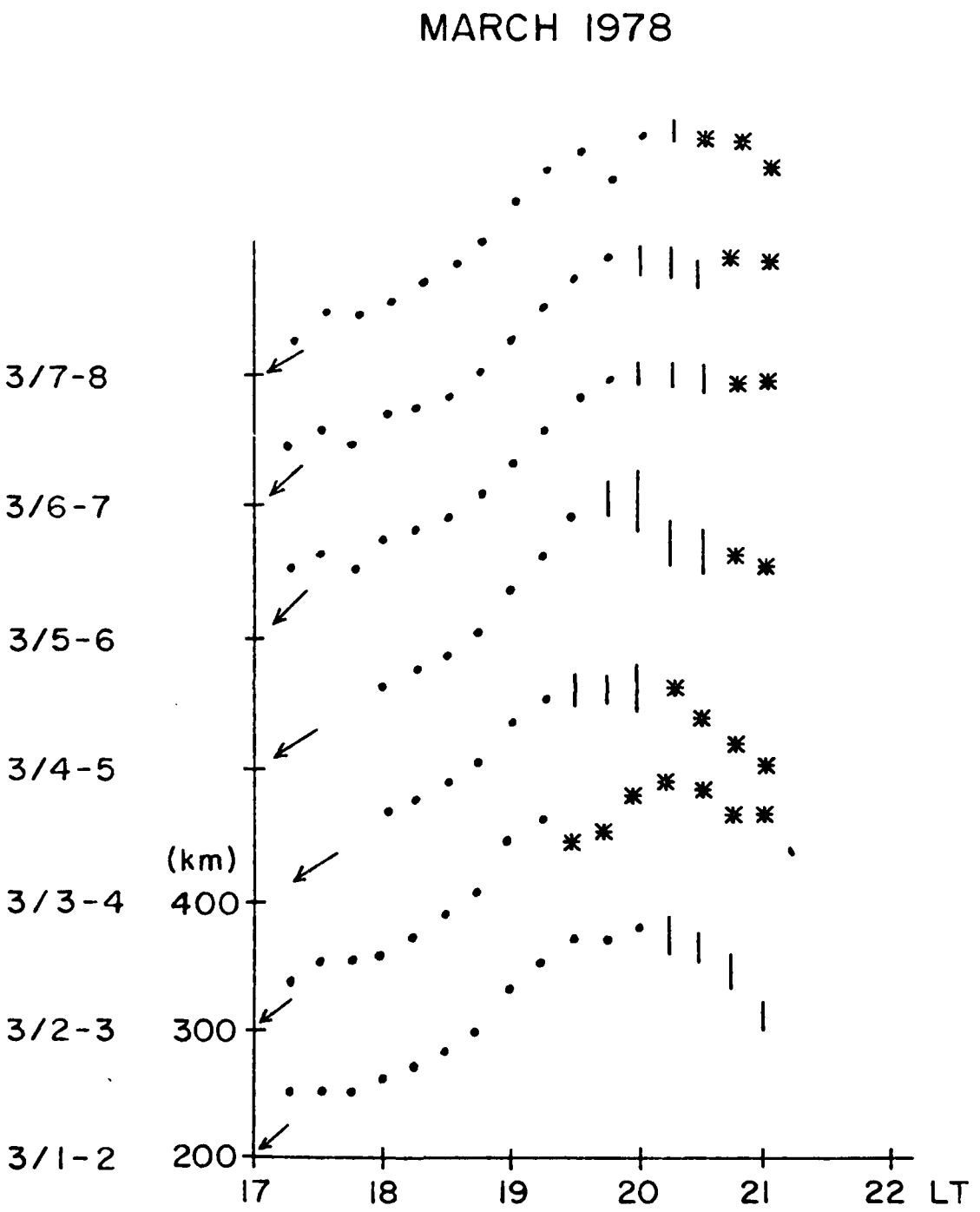
MARCH 1978
3/7-8
3/6-7
3/5-6
3/4-5
3/3-4
3/2-3
3/1-2
(km)
400
300
200
17
18
19
20
21
22
LT

Figure 2d

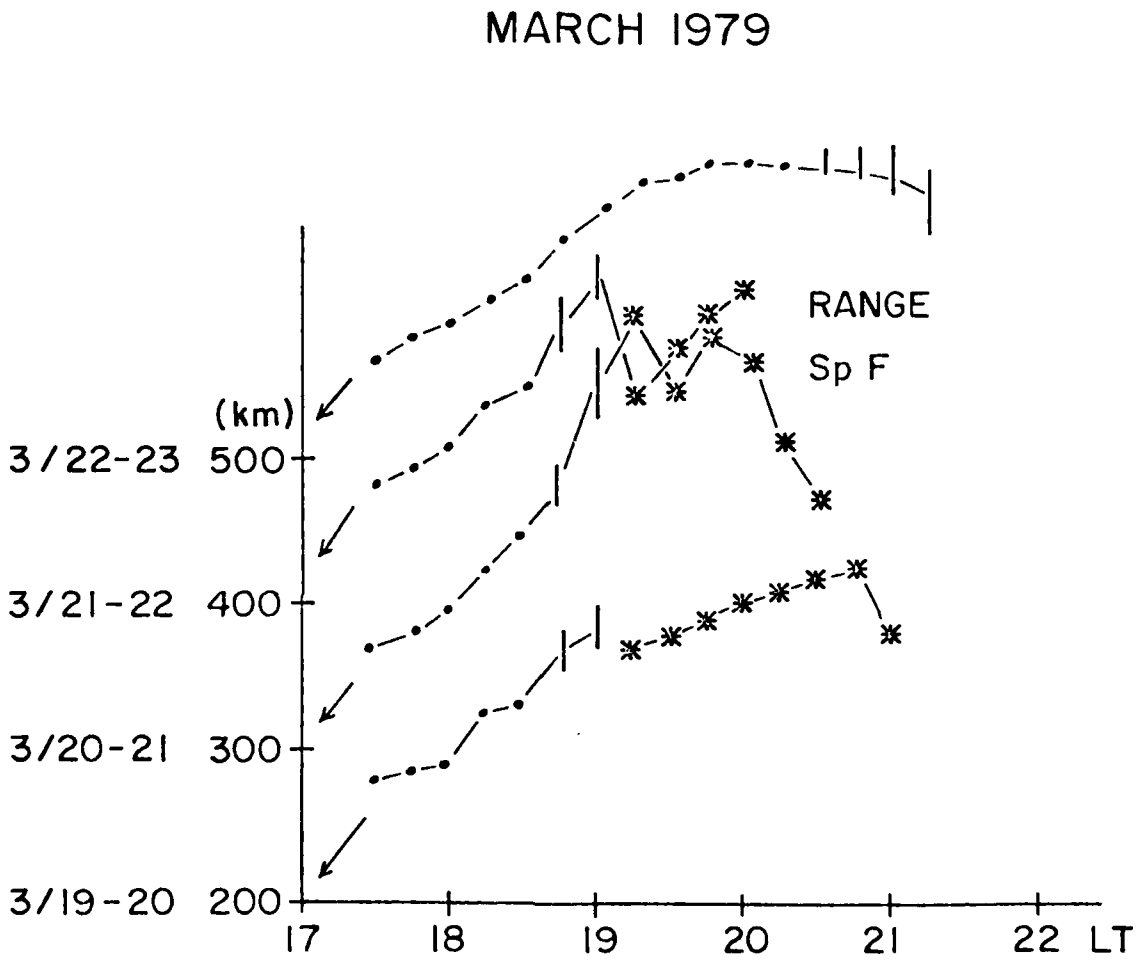
MARCH 1979
RANGE
Sp F
(km)
3/22-23
3/21-22
3/20-21
3/19-20
500
400
300
200
17
18
19
20
21
22
LT

Figure 2e

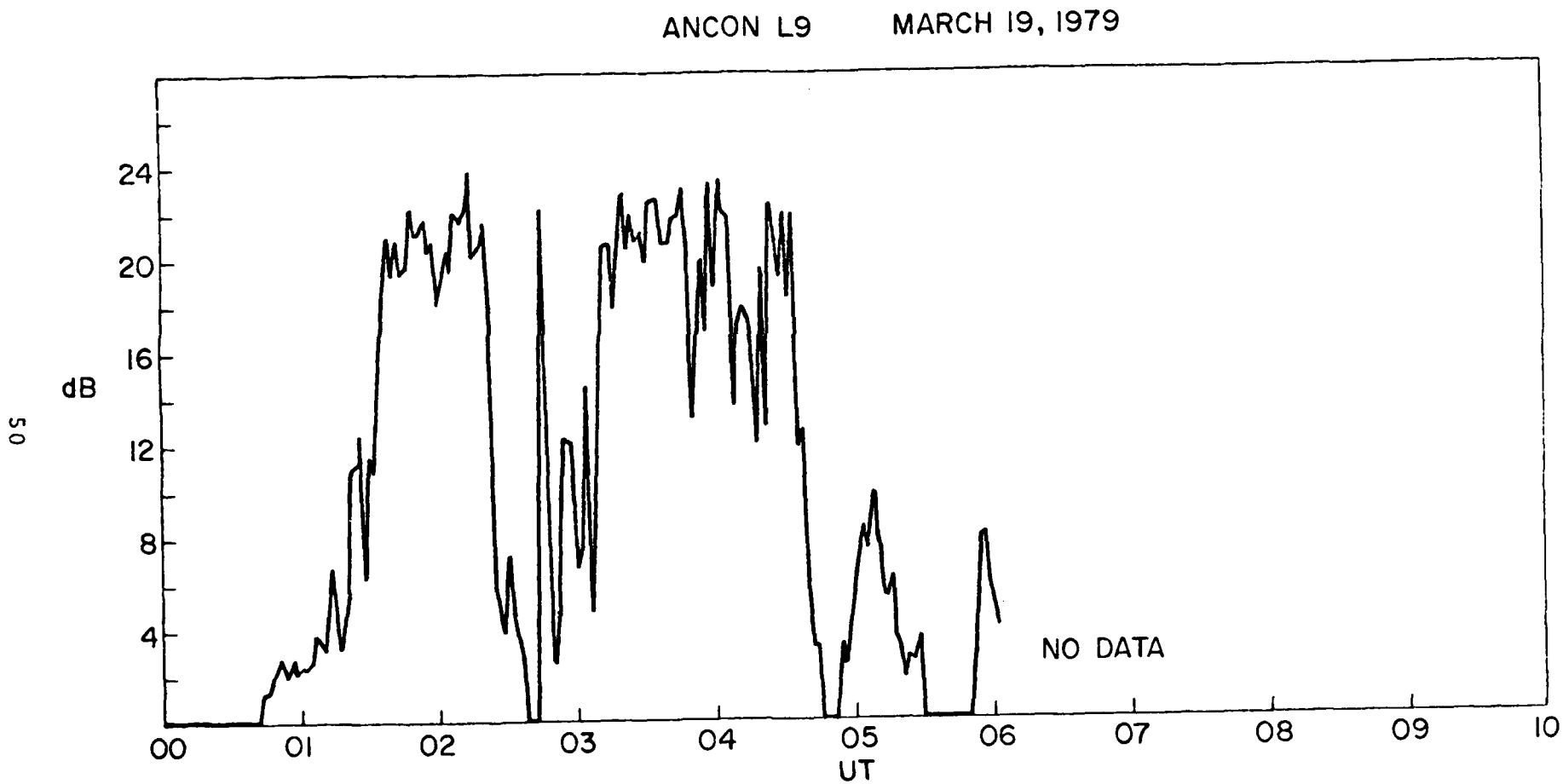
ANCON L9 MARCH 19, 1979
dB
24
20
16
12
8
4
50
00
01
02
03
04
05
06
07
08
09
10
UT
NO DATA

Figure 3a

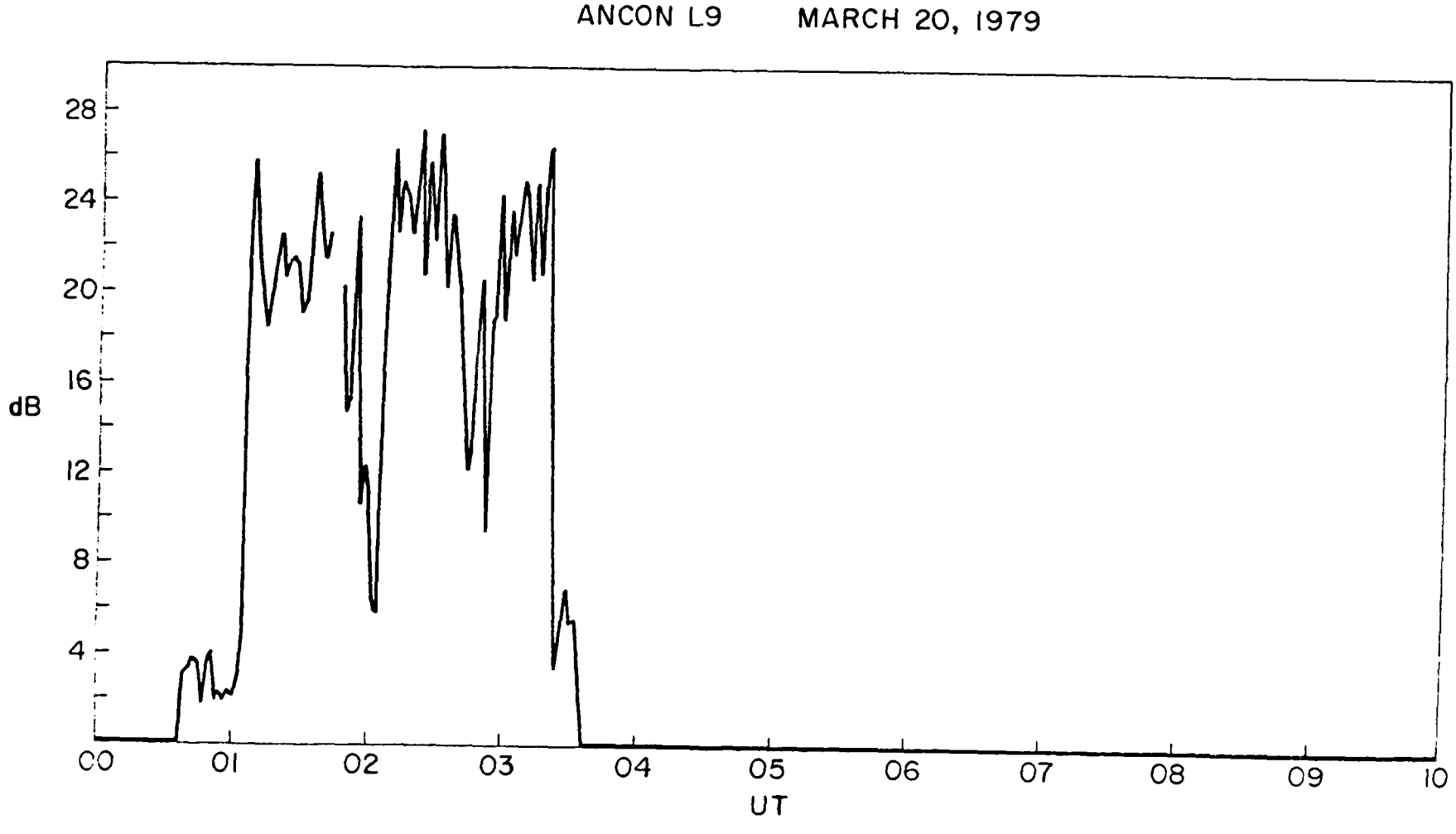
ANCON L9 MARCH 20, 1979
dB
28
24
20
16
12
8
4
00
01
02
03
04
05
06
07
08
09
10
UT

Figure 3b

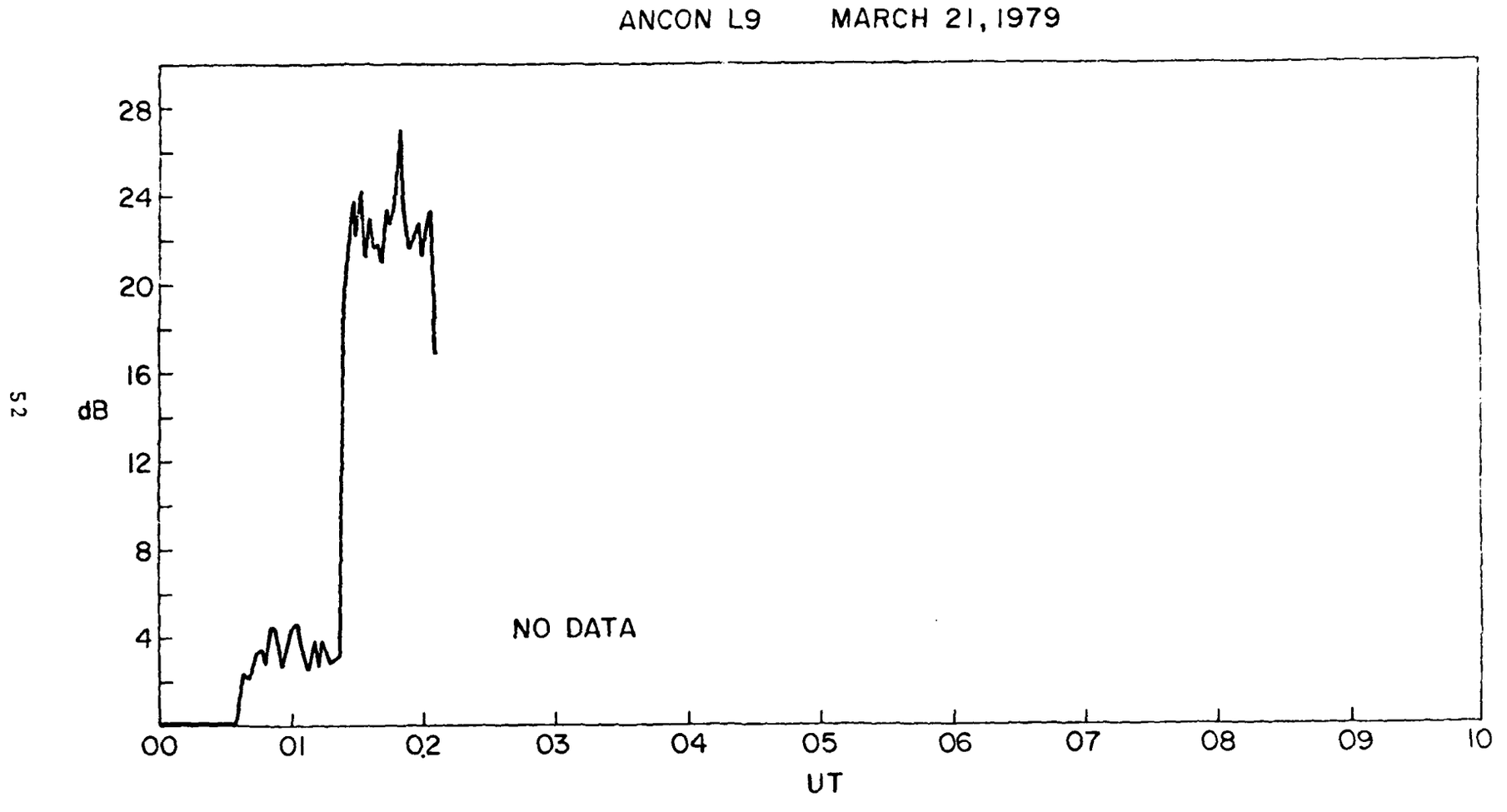
ANCON L9 MARCH 21, 1979
28
24
20
16
12
8
4
dB
NO DATA
00
01
02
03
04
05
06
07
08
09
10
UT

Figure 3c

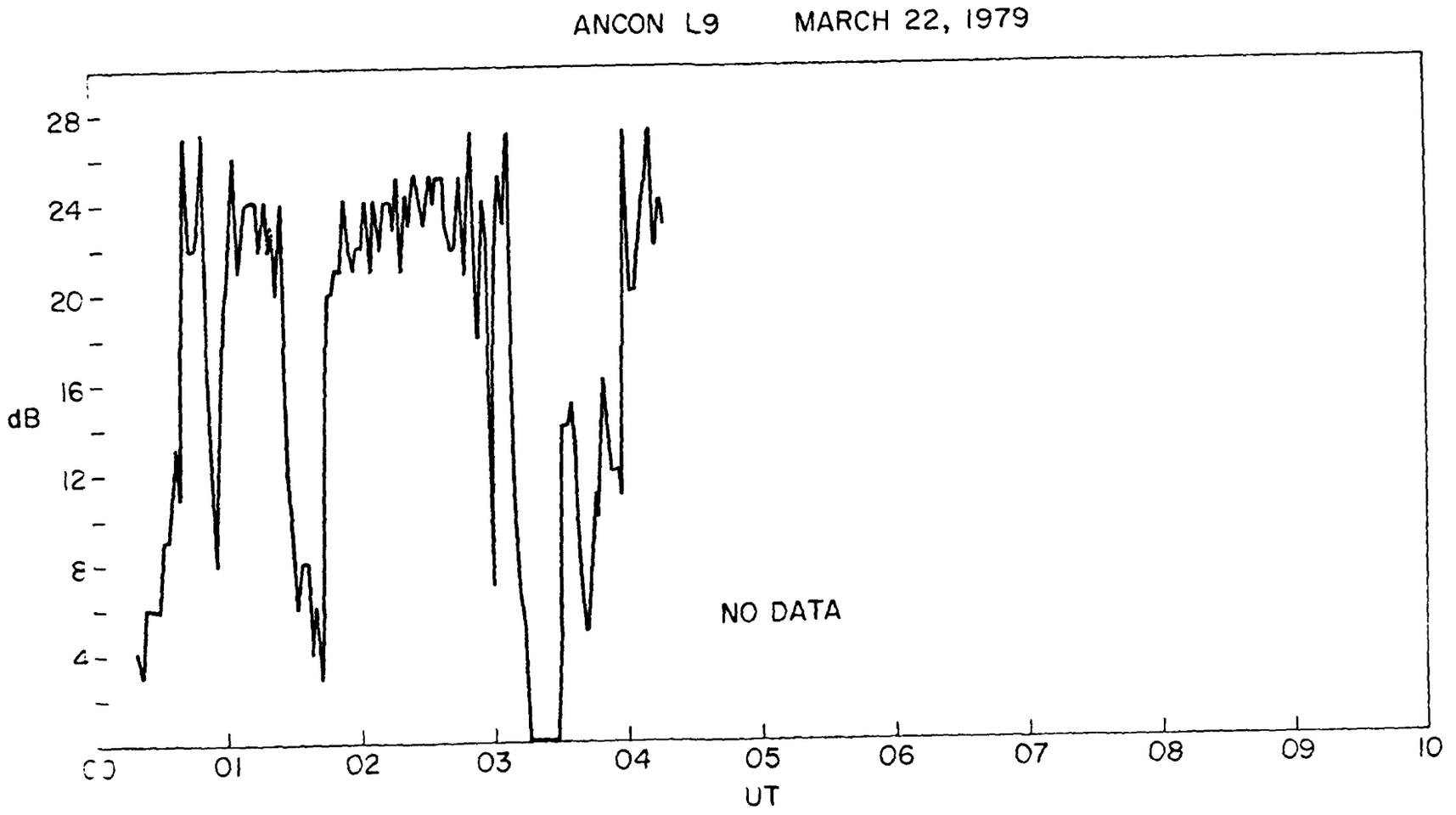
ANCON L9 MARCH 22, 1979
28
24
20
16
12
8
4
dB
NO DATA
00
01
02
03
04
05
06
07
08
09
10
UT

Figure 3d

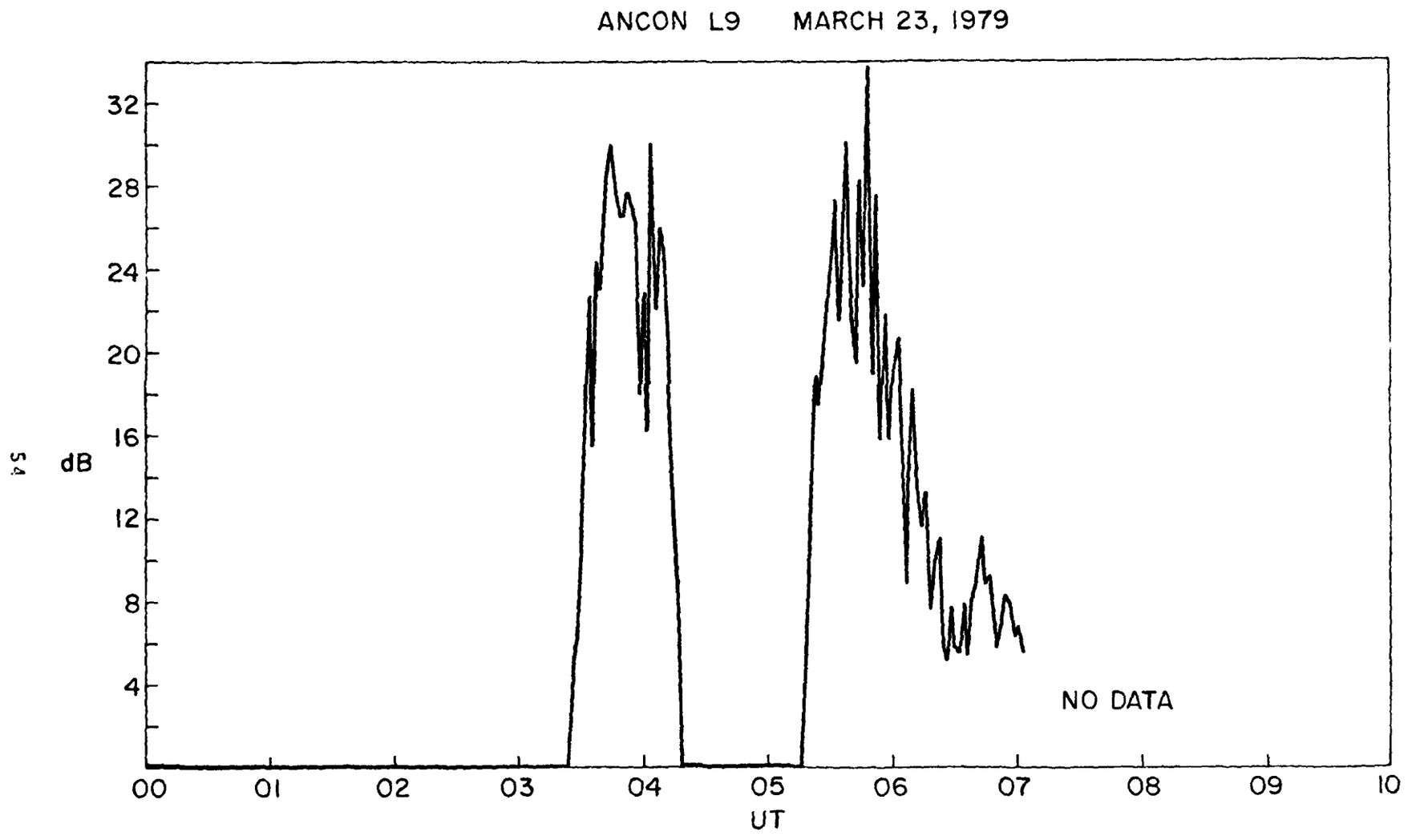
ANCON L9 MARCH 23, 1979
32
28
24
20
16
12
8
4
dB
NO DATA
00
01
02
03
04
05
06
07
08
09
10
UT

Figure 3e

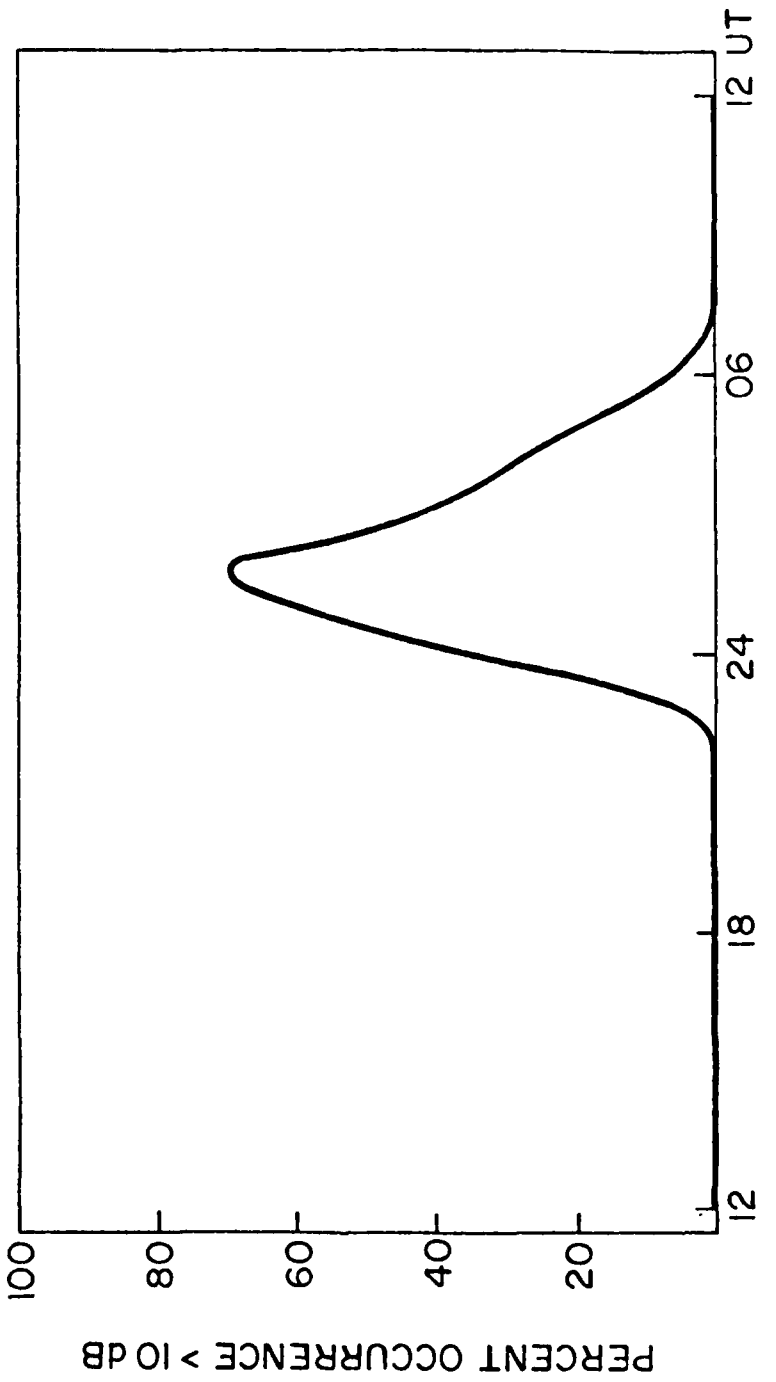
ANCON L9 MARCH 1977
PERCENT OCCURRENCE > 10 dB
100
80
60
40
20
12
18
24
06
12 UT

Figure 4a

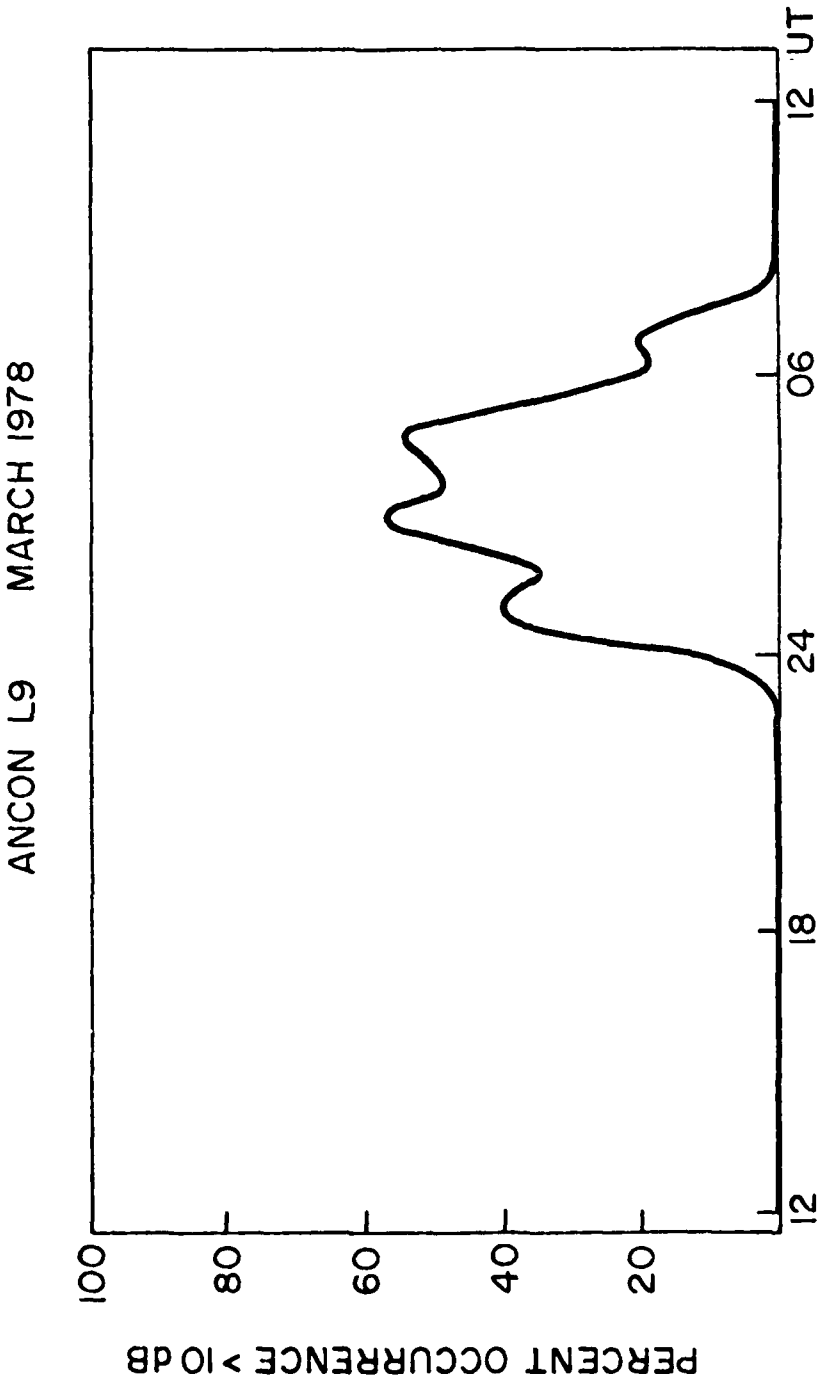
ANCON L9 MARCH 1978
PERCENT OCCURRENCE > 10 dB
100
80
60
40
20
12
18
24
06
12 UT

Figure 4b

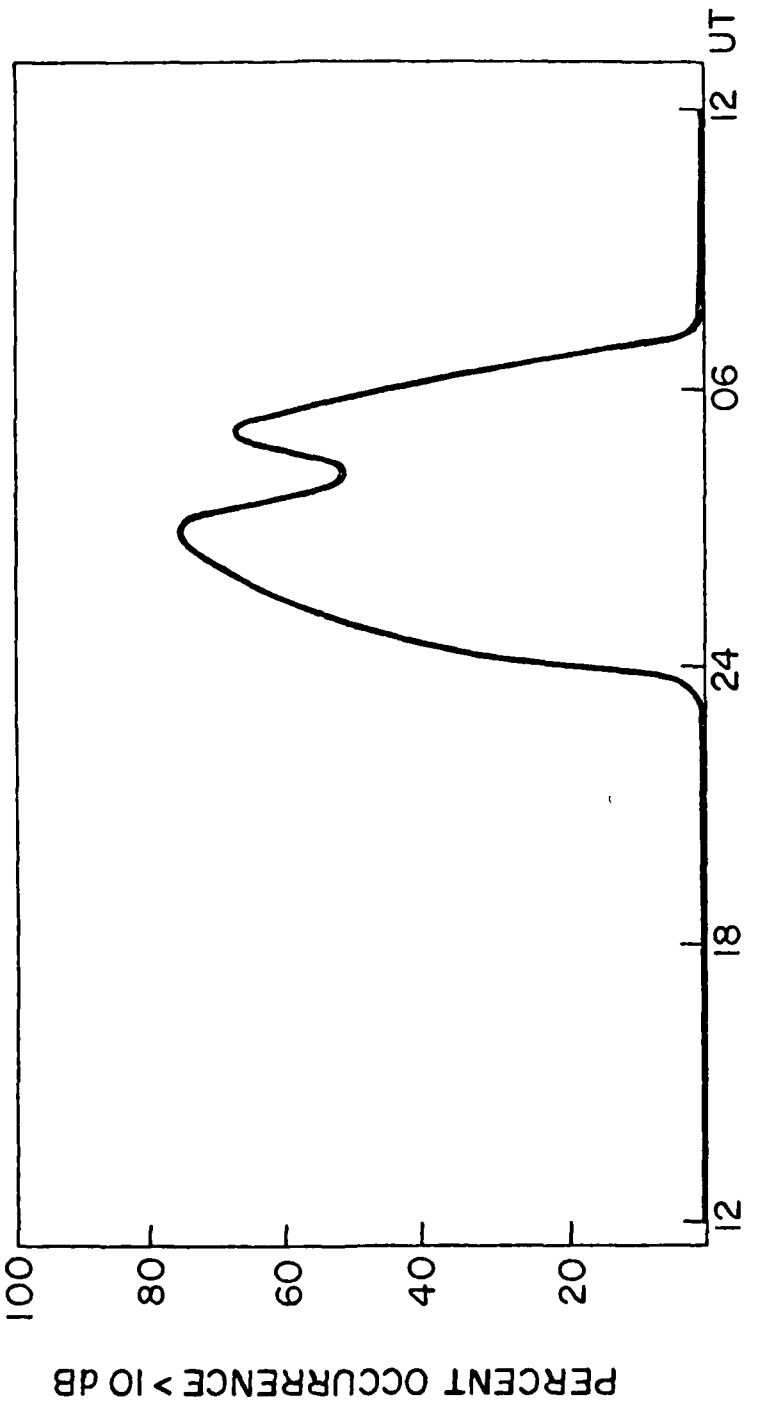
ANCON L9 MARCH 1979
PERCENT OCCURRENCE > 10 dB
100
80
60
40
20
12
18
24
06
12 UT

Figure 4c

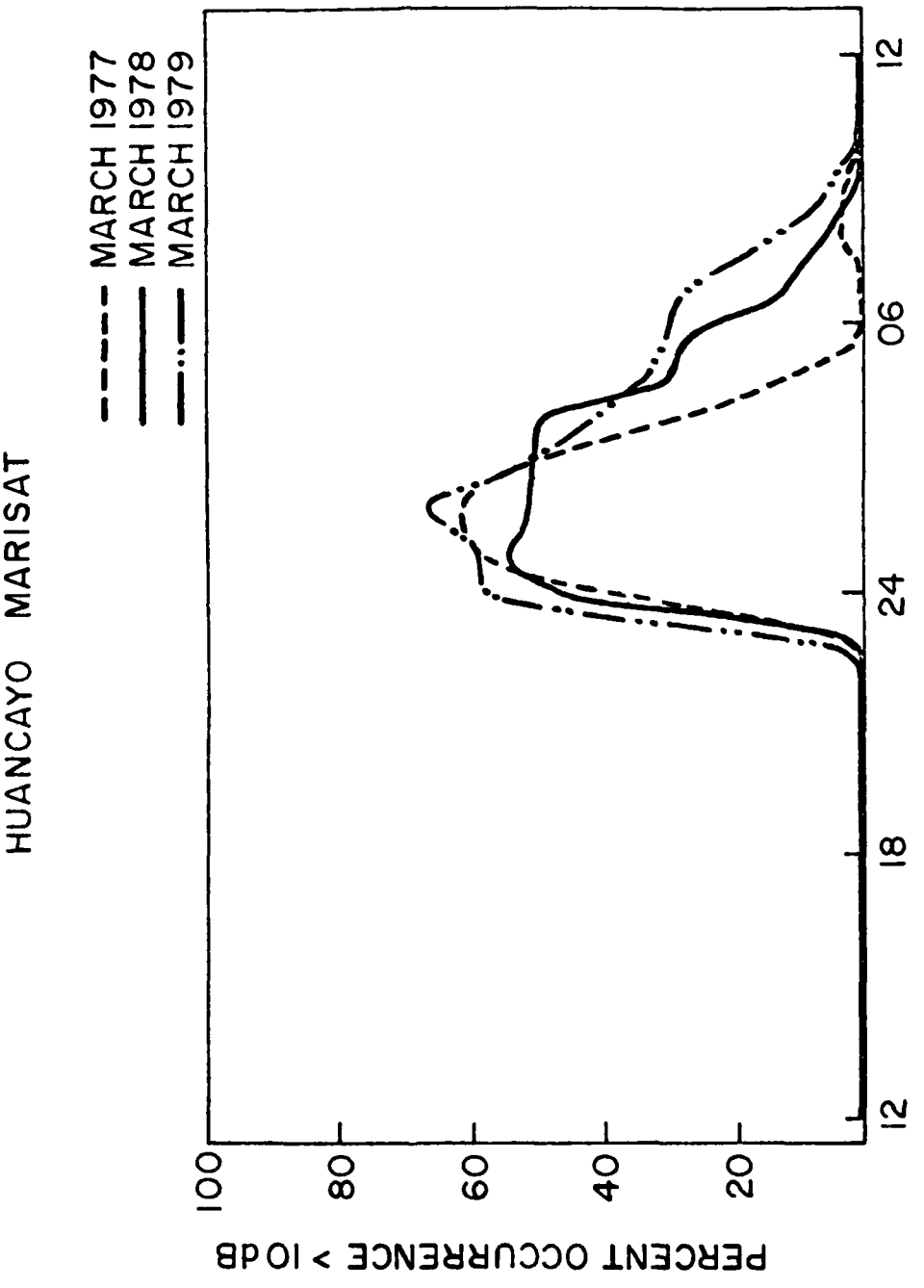
HUANCAYO MARISAT
MARCH 1977
MARCH 1978
MARCH 1979
PERCENT OCCURRENCE > 10 dB
100
80
60
40
20
12
18
24
UT
06
12

Figure 5

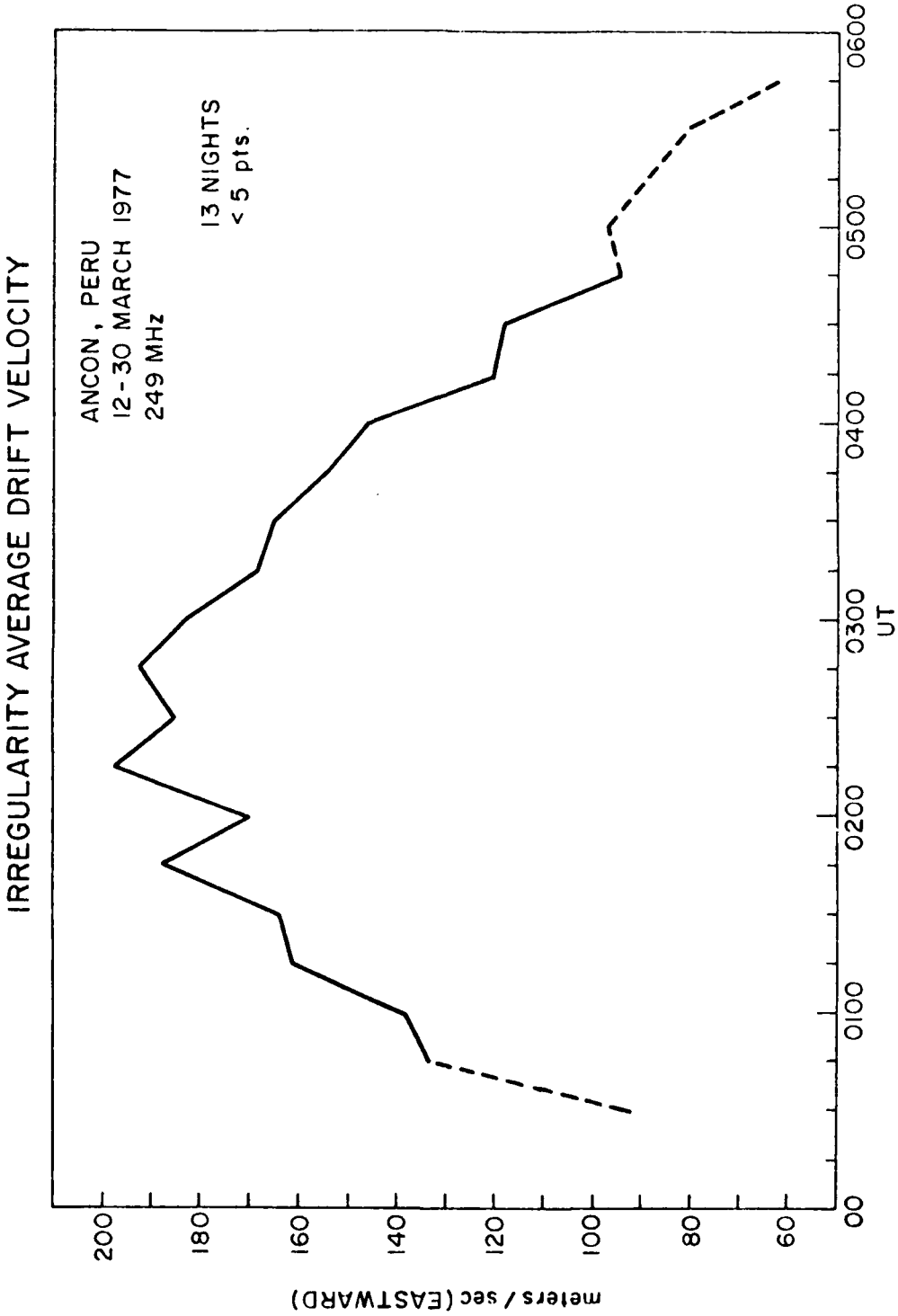
IRREGULARITY AVERAGE DRIFT VELOCITY
ANCON, PERU
12-30 MARCH 1977
249 MHz
13 NIGHTS
< 5 pts.
meters / sec (EASTWARD)
200
180
160
140
120
100
80
60
00
0100
0200
0300
0400
0500
0600
UT

Figure 6a

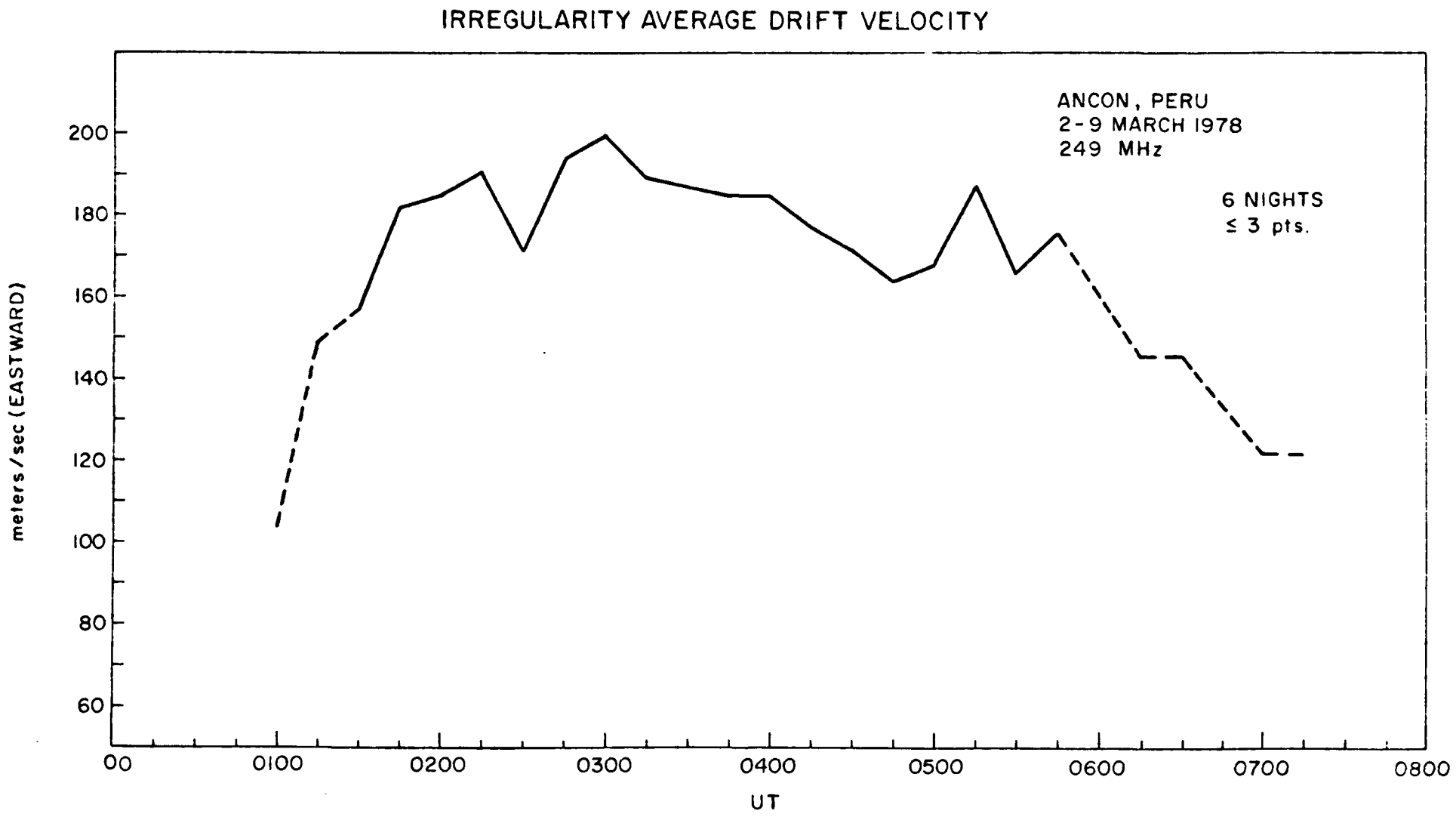
IRREGULARITY AVERAGE DRIFT VELOCITY
ANCON, PERU
2-9 MARCH 1978
249 MHz
6 NIGHTS
≤ 3 pts.
meters/sec (EASTWARD)
200
180
160
140
120
100
80
60
00
0100
0200
0300
0400
0500
0600
0700
0800
UT

Figure 6b

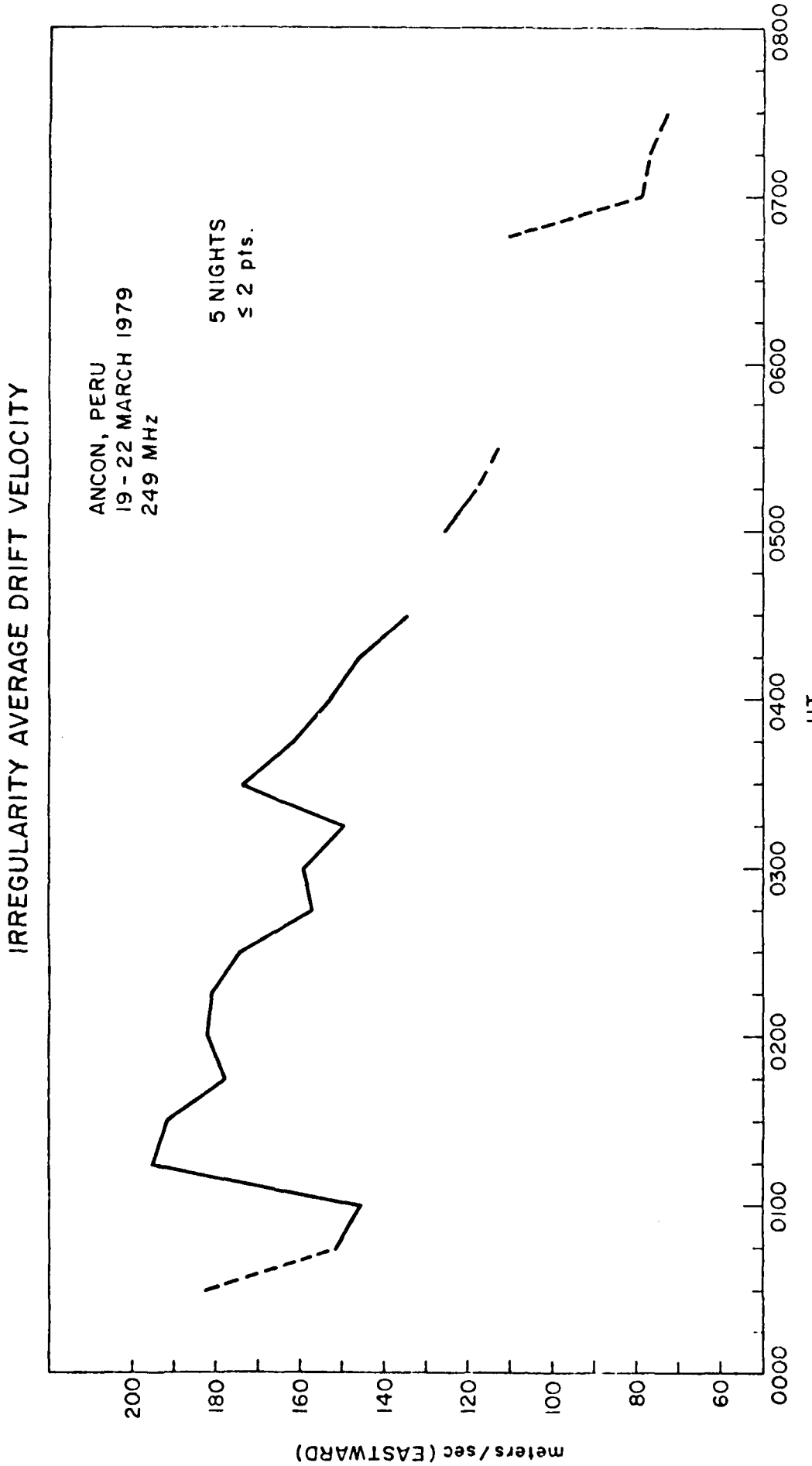
IRREGULARITY AVERAGE DRIFT VELOCITY
ANCON, PERU
19 - 22 MARCH 1979
249 MHz
5 NIGHTS
≤ 2 pts.
meters/sec (EASTWARD)
200
180
160
140
120
100
80
60
0000
0100
0200
0300
0400
0500
0600
0700
0800
UT

Figure 6c

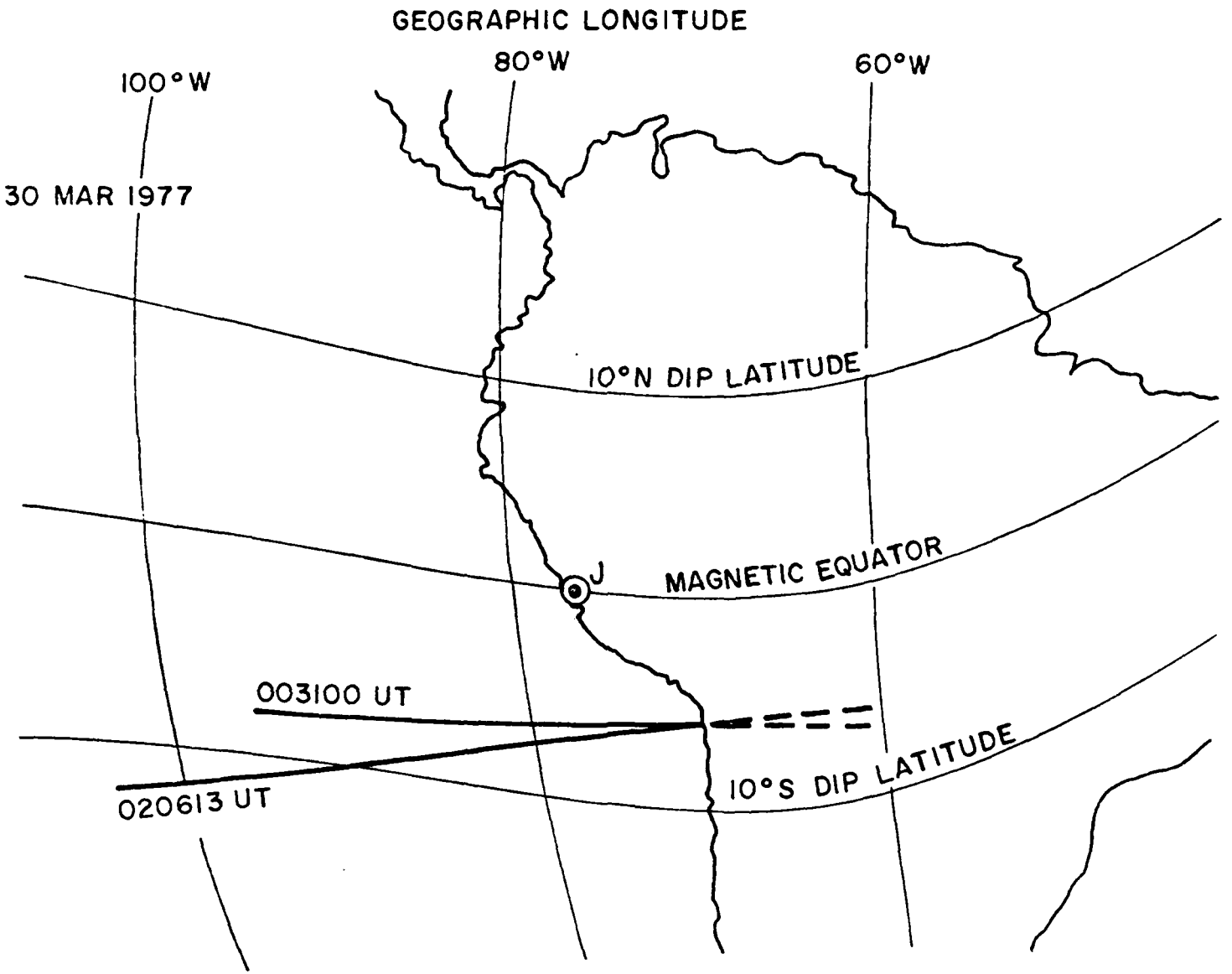
GEOGRAPHIC LONGITUDE
100°W
80°W
60°W
30 MAR 1977
10°N DIP LATITUDE
J
MAGNETIC EQUATOR
003100 UT
020613 UT
10°S DIP LATITUDE

Figure 7

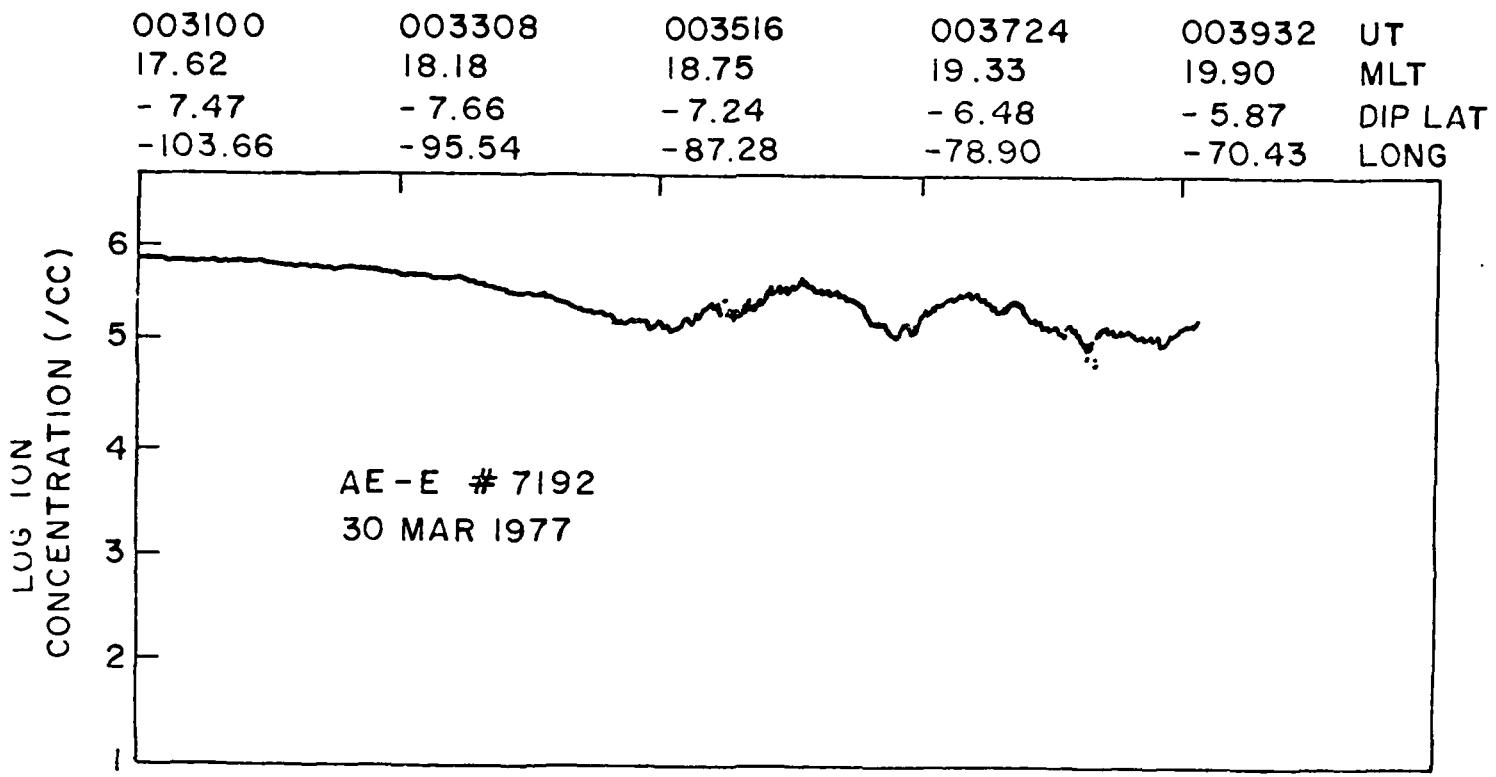
003100
17.62
- 7.47
-103.66
003308
18.18
- 7.66
-95.54
003516
18.75
- 7.24
-87.28
003724
19.33
- 6.48
-78.90
003932
19.90
- 5.87
-70.43
UT
MLT
DIP LAT
LONG
LOG ION CONCENTRATION (/CC)
6
5
4
3
2
1
AE-E #7192
30 MAR 1977

Figure 8

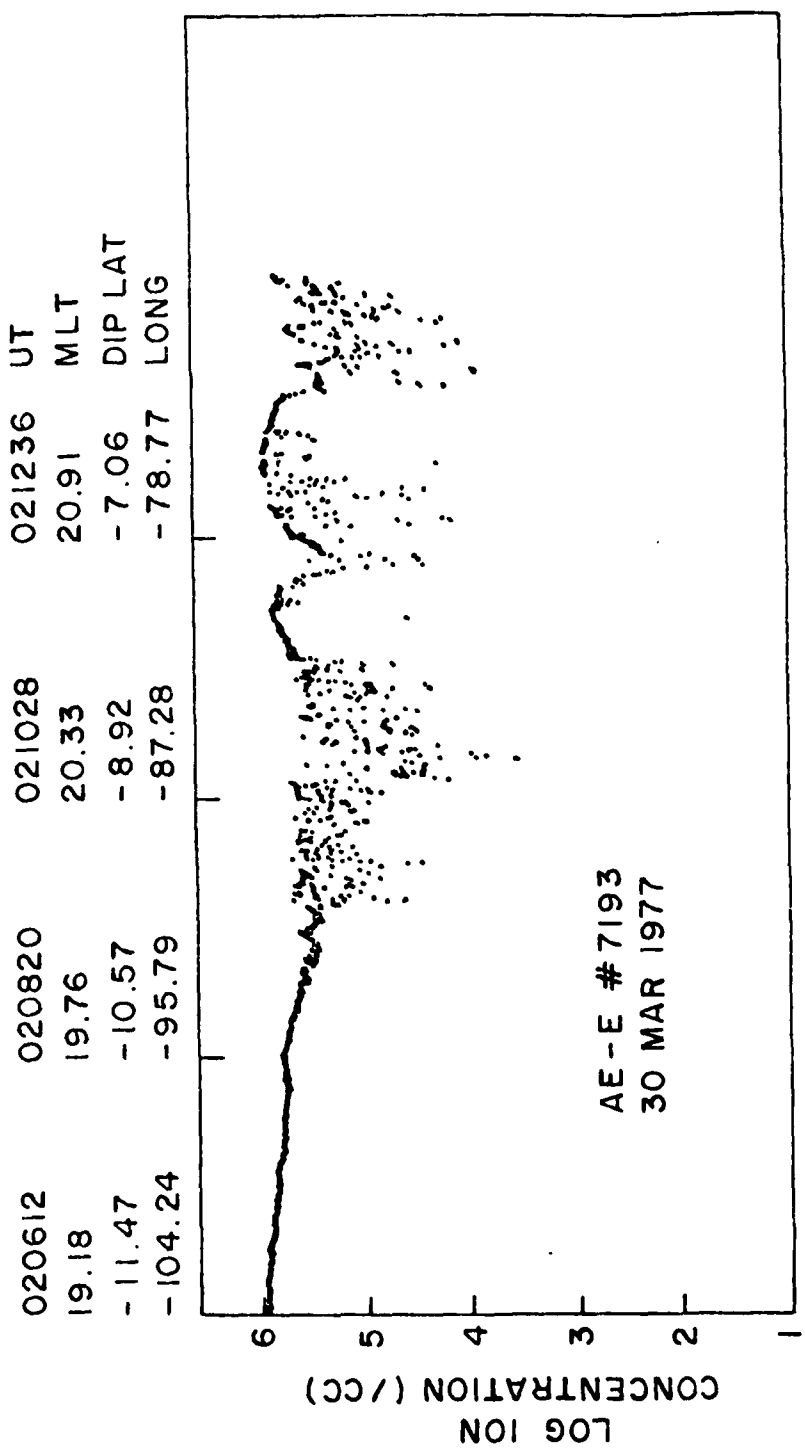
020612 020820 021028 021236 UT
19.18 19.76 20.33 20.91 MLT
-11.47 -10.57 -8.92 -7.06 DIP LAT
-104.24 -95.79 -87.28 -78.77 LONG
AE-E #7193
30 MAR 1977
LOG ION CONCENTRATION (/CC)
6
5
4
3
2
1

Figure 9

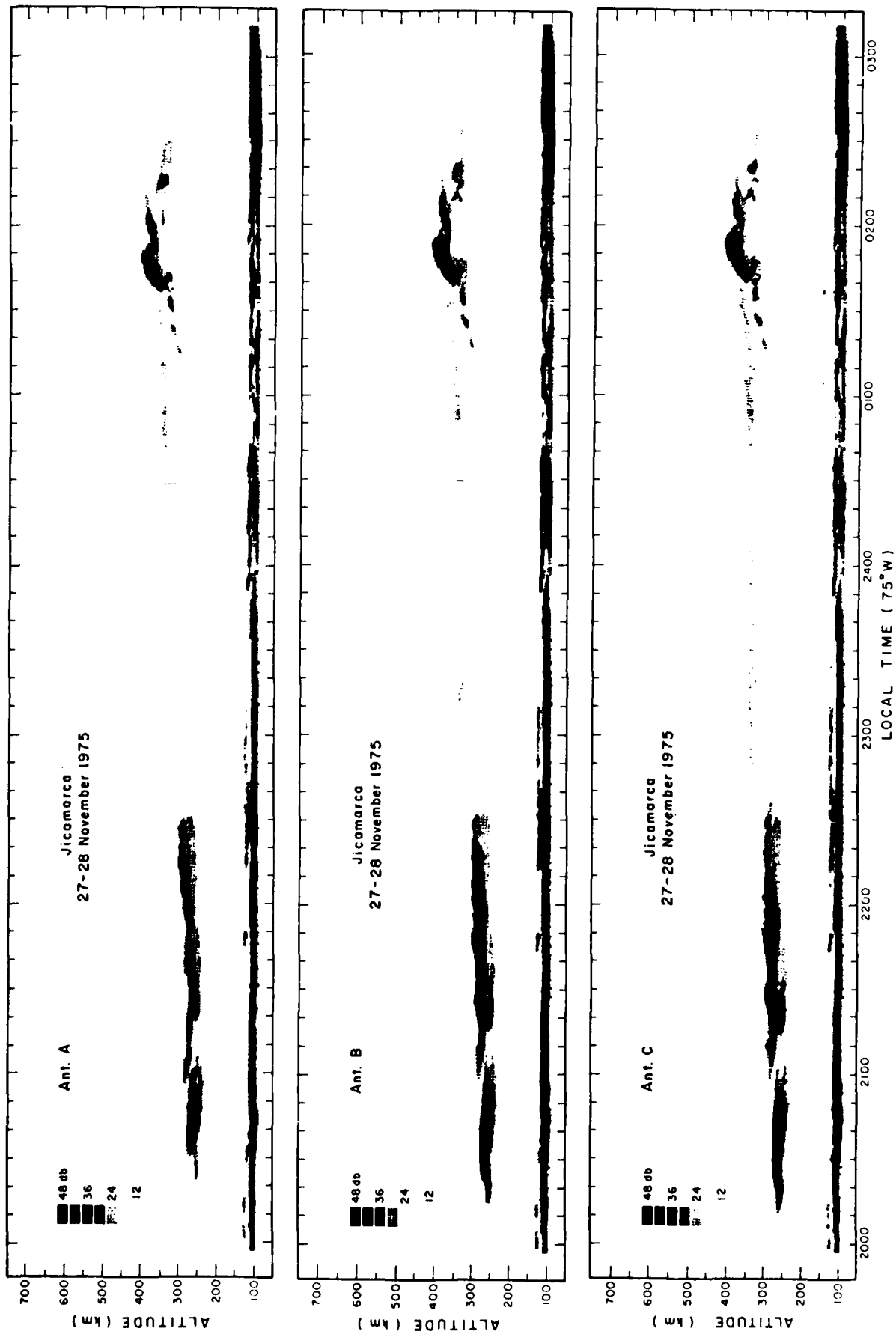
Ant. A
Jicamarca
27-28 November 1975
48 db
36
24
12
Ant. B
Jicamarca
27-28 November 1975
48 db
36
24
12
Ant. C
Jicamarca
27-28 November 1975
48 db
36
24
12
ALTITUDE (km)
700
600
500
400
300
200
100
2000
2100
2200
2300
2400
0100
0200
0300
LOCAL TIME (75°W)

Figure 10a

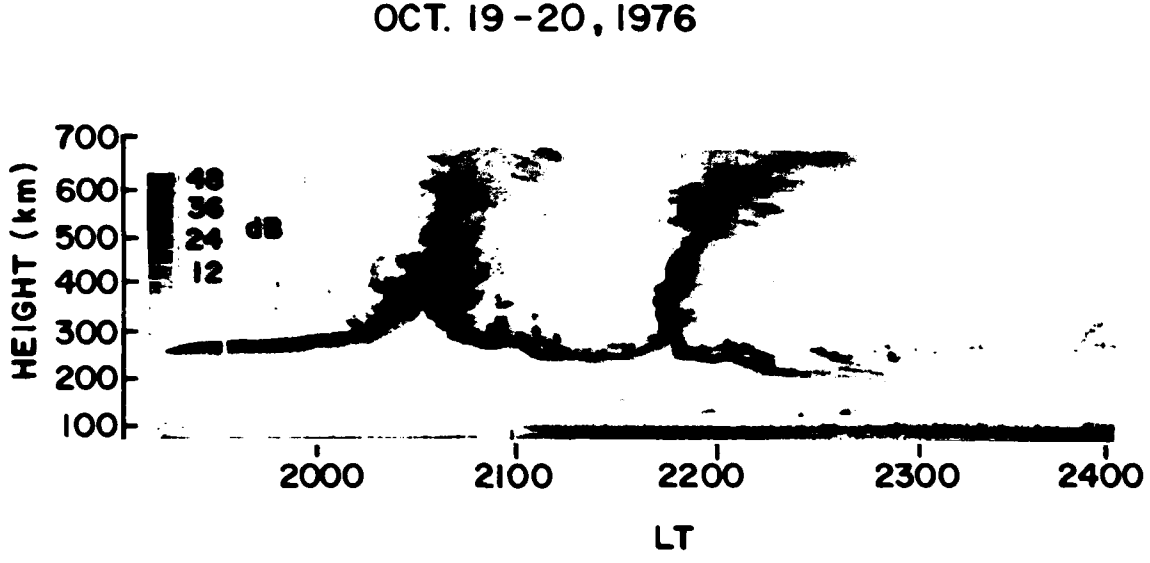
OCT. 19-20, 1976
HEIGHT (km)
700
600
500
400
300
200
100
48
36
24
12
dB
2000
2100
2200
2300
2400
LT

Figure 10b

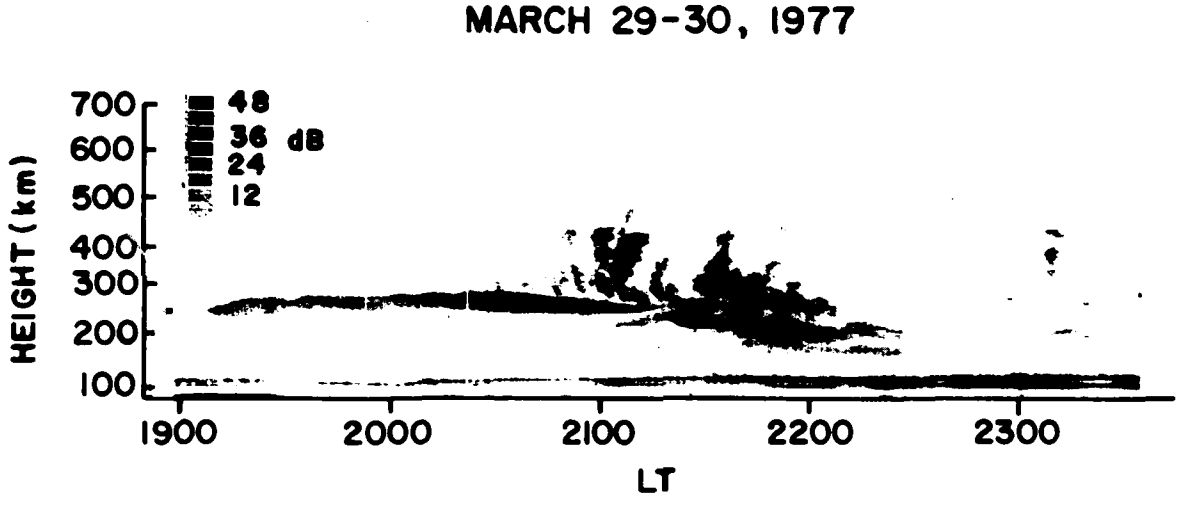
MARCH 29-30, 1977
HEIGHT (km)
700
600
500
400
300
200
100
48
36
24
12
dB
1900
2000
2100
2200
2300
LT

Figure 10c

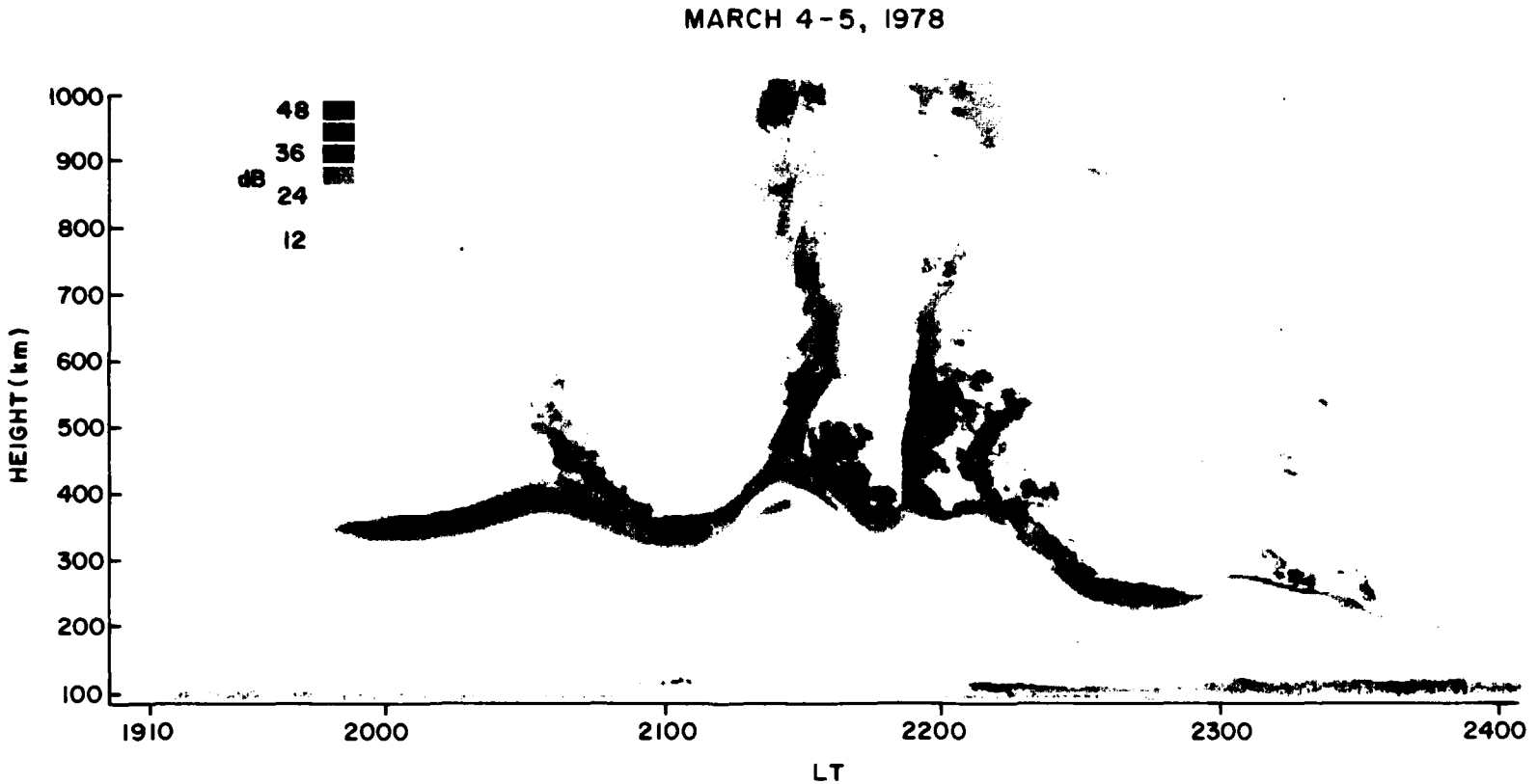
MARCH 4-5, 1978
HEIGHT (km)
1000
900
800
700
600
500
400
300
200
100
dB
48
36
24
12
1910
2000
2100
2200
2300
2400
LT

Figure 10d

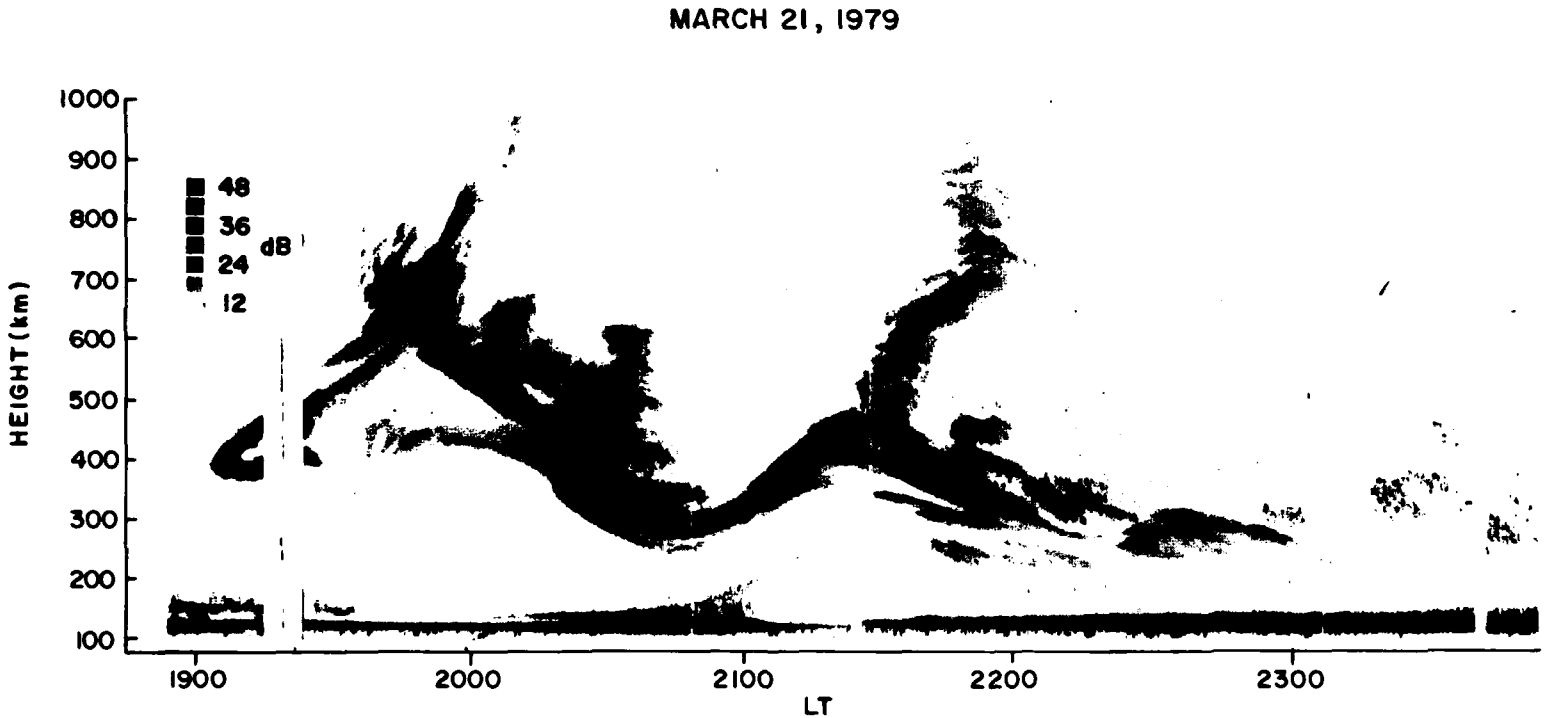
MARCH 21, 1979
HEIGHT (km)
1000
900
800
700
600
500
400
300
200
100
48
36
24
12
dB
1900
2000
2100
2200
2300
LT

Figure 10e

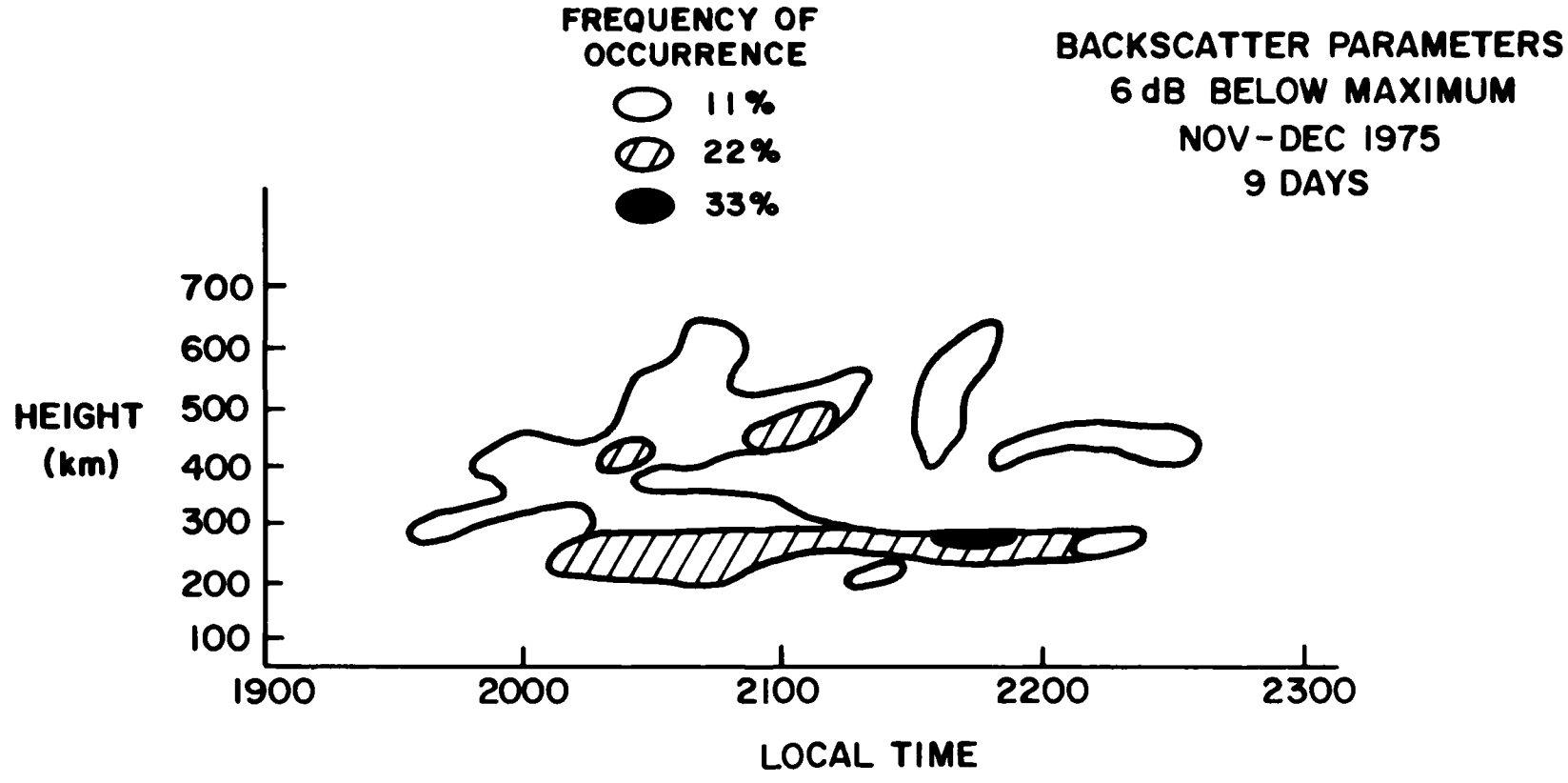
FREQUENCY OF
OCCURRENCE
11%
22%
33%
BACKSCATTER PARAMETERS
6 dB BELOW MAXIMUM
NOV-DEC 1975
9 DAYS
HEIGHT
(km)
700
600
500
400
300
200
100
1900
2000
2100
2200
2300
LOCAL TIME

Figure 11a

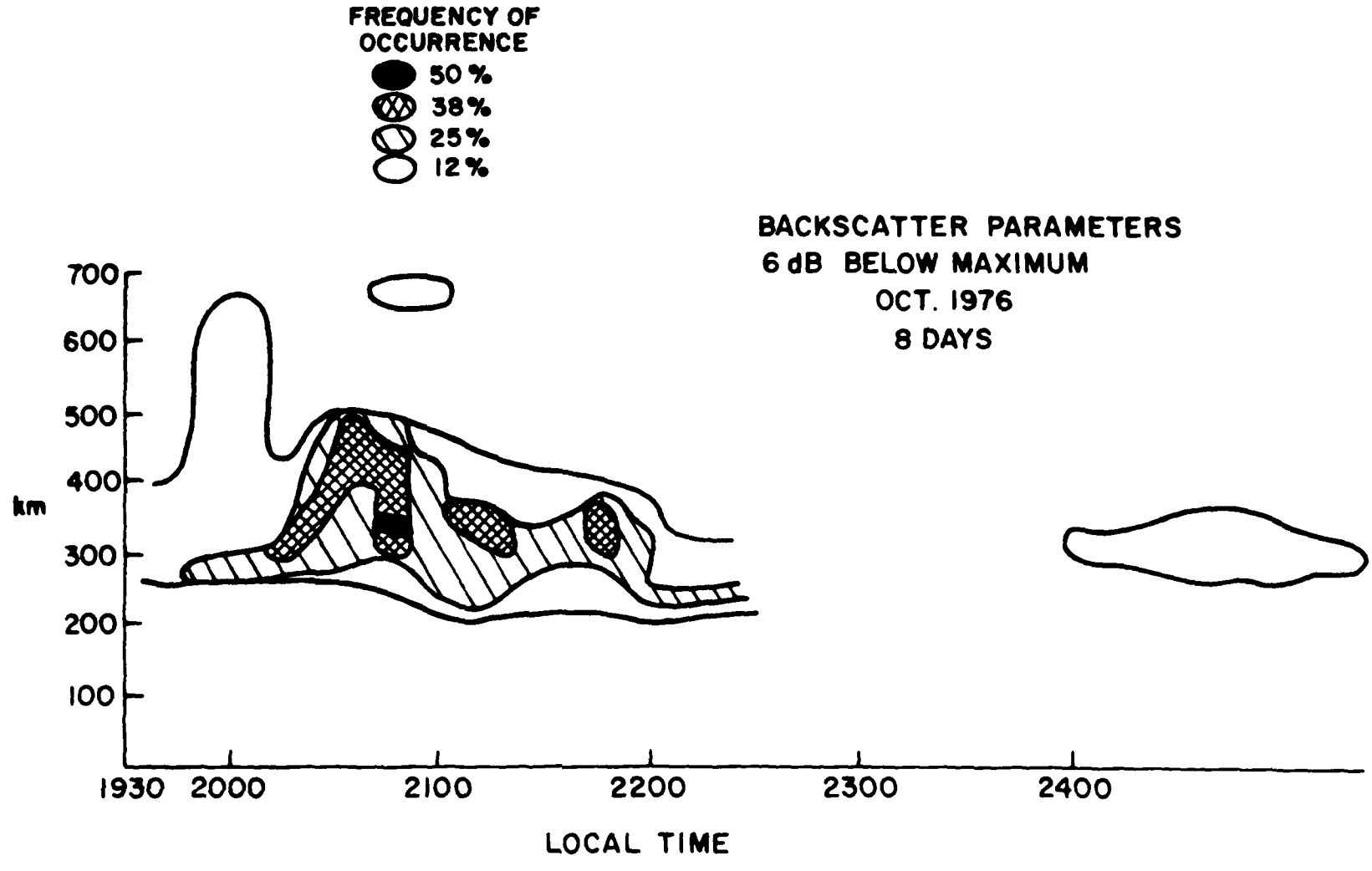
FREQUENCY OF
OCCURRENCE
50 %
38%
25%
12%
BACKSCATTER PARAMETERS
6 dB BELOW MAXIMUM
OCT. 1976
8 DAYS
700
600
500
400
300
200
100
km
1930
2000
2100
2200
2300
2400
LOCAL TIME

Figure 11b

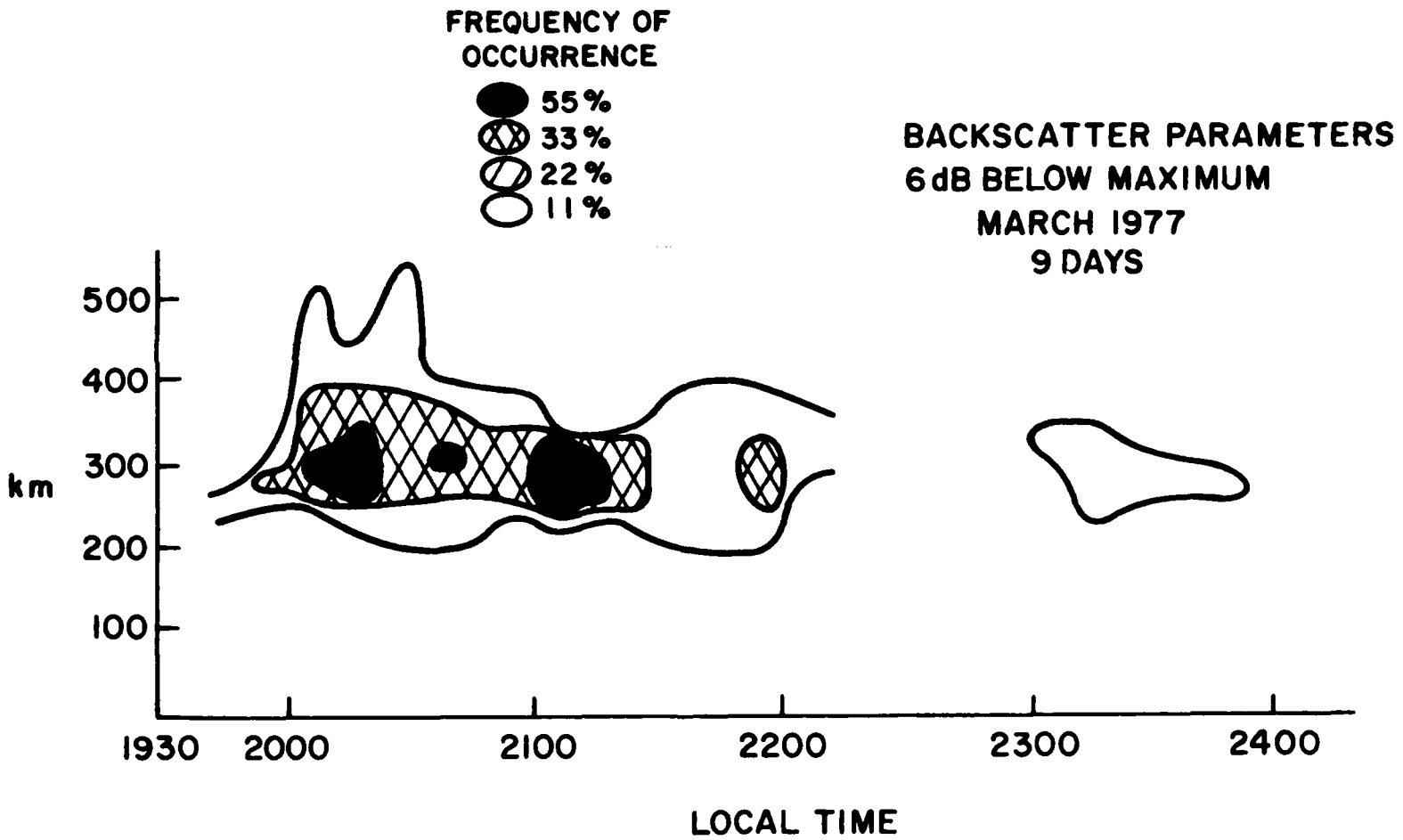
FREQUENCY OF
OCCURRENCE
55%
33%
22%
11%
BACKSCATTER PARAMETERS
6dB BELOW MAXIMUM
MARCH 1977
9 DAYS
500
400
300
200
100
km
1930
2000
2100
2200
2300
2400
LOCAL TIME

Figure 11c

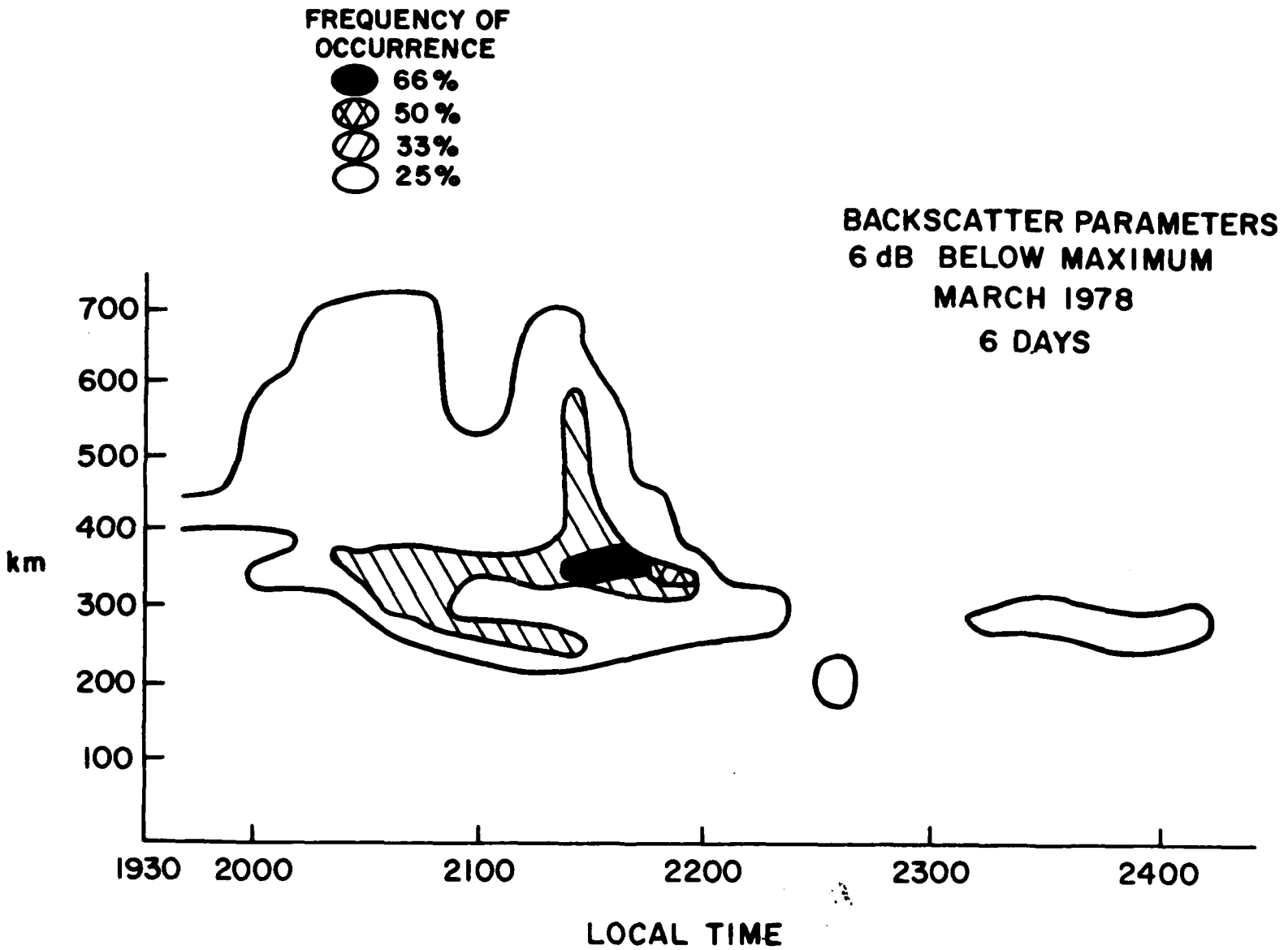
FREQUENCY OF
OCCURRENCE
66%
50%
33%
25%
BACKSCATTER PARAMETERS
6 dB BELOW MAXIMUM
MARCH 1978
6 DAYS
700
600
500
400
300
200
100
km
1930
2000
2100
2200
2300
2400
LOCAL TIME

Figure 11d

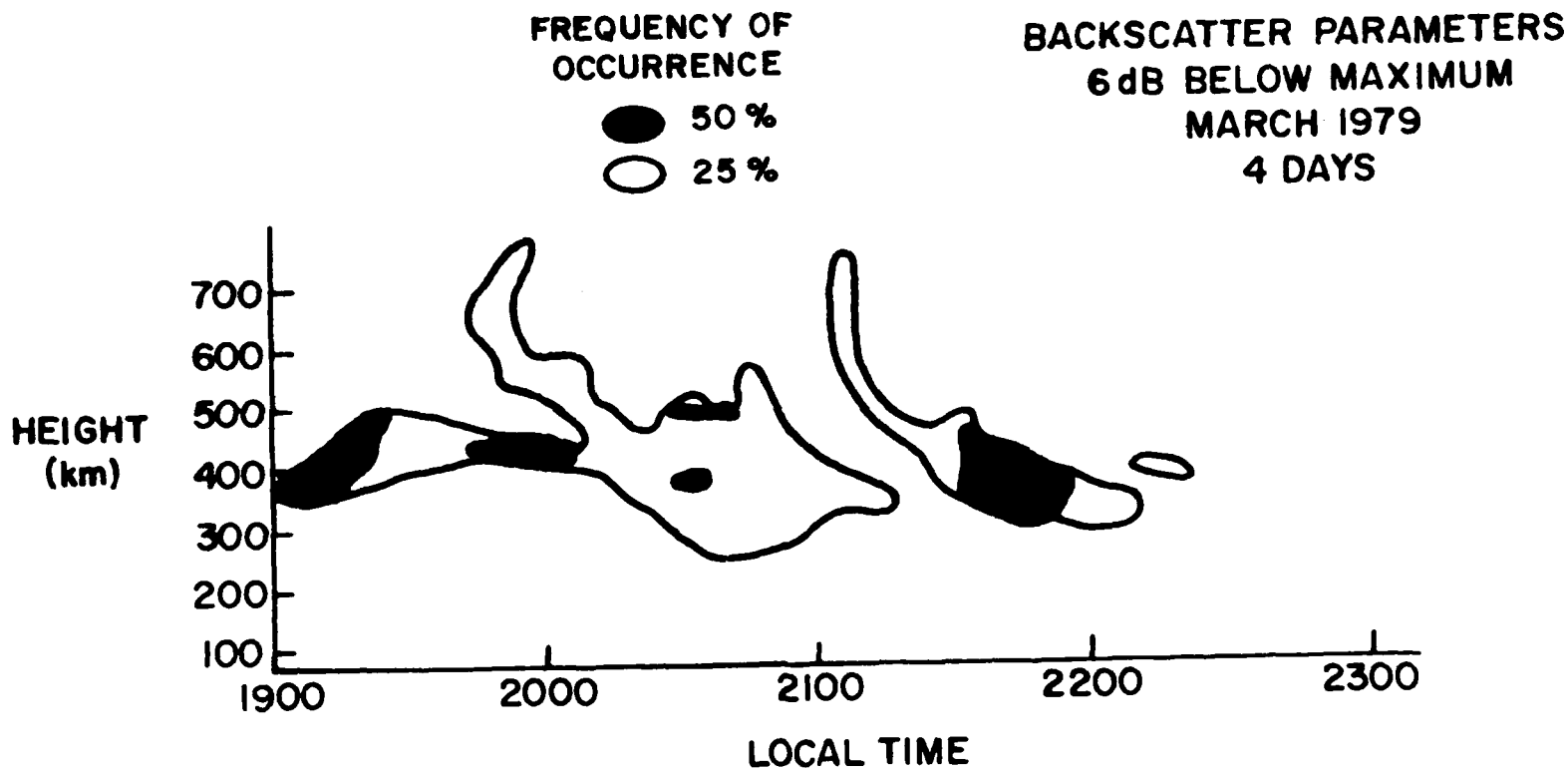
FREQUENCY OF
OCCURRENCE
50 %
25 %
BACKSCATTER PARAMETERS
6 dB BELOW MAXIMUM
MARCH 1979
4 DAYS
HEIGHT
(km)
700
600
500
400
300
200
100
1900
2000
2100
2200
2300
LOCAL TIME

Figure 11e

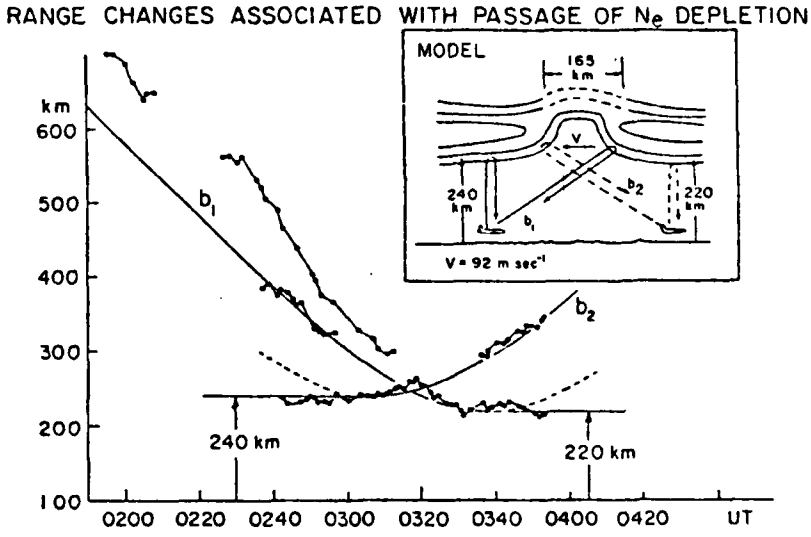
RANGE CHANGES ASSOCIATED WITH PASSAGE OF N_e DEPLETION
MODEL
165 km
V
240 km
220 km
b_2
b_1
V = 92 m sec^{-1}
km
600
500
400
300
200
100
b_1
b_2
240 km
220 km
0200
0220
0240
0300
0320
0340
0400
0420
UT

Figure 12

DNA Distribution List

Berkeley Research Assoc.
Attn: Clifford W. Prettie
P.O. Box 983
Berkeley, CA 94701

ESL, Inc.
Attn: J. Marshall
495 Java Drive
Sunnyvale, CA 94086

Def. Nuclear Agency
Attn: STTL Tech. Library
Washington, D.C. 20305

Mission Research Corp.
Attn: R. Bogush
735 State St.
Santa Barbara, CA 93101

Naval Research Lab.
Attn: Dr. John Goodman
Code 4110
Washington, D.C. 20375

Dr. Jules Aarons
Dept. of Astronomy
Boston University
Boston, MA 02215

Major G. Wortham
AFGWC/WSE
Offutt AFB, NE 68113

Lt. P. Styczek
SAC/CA/CSS
Offutt AFB, NE 68113

Ed Skomal
Aerospace Corp.
Box 92957
Los Angeles, CA 90009

Allen L. Johnson
Air Force Avionics Lab
AFAL/AAAI
Wright Patterson AFB
Ohio 45433

Dow Evelyn
Def Nuclear Agency/RAAE
Washington, D.C. 20305

Major L. Wittwer
Def Nuclear Agency/RAAE
Washington, D.C. 20305

Major R. Sutton
SD/YKX
P.O. Box 92960
Worldway Postal Center
Los Angeles, CA 90009

Dr. H. Soicher
US Army Communication Res. and
Development Commons
Fort Monmouth, N.J. 07703
(DRDCO-COM-RH-4)

SRI International
333 Ravenswood Ave.
Menlo Park, CA 94025
Attn: C. Rino

SRI International
333 Ravenswood Ave.
Menlo Park CA 94025
Attn: James Vickrey

SRI International
333 Ravenswood Ave.
Menlo Park CA 94025
Attn: Roland T. Tsunoda

SRI International
333 Ravenswood Ave.
Menlo Park, CA 94025
Attn: R. Livingston

Physical Dynamics, Inc.
P.O. Box 3027
Bellevue, WA 98009
Attn: E.J. Fremouw

Dr. K. Davies
NOAA
Boulder, CO 80302

Code 427
Dept. of the Navy
Office of Naval Research
Arlington, VA 22217

Dr. George Millman
General Electric Co.
Building 9, Room 46
Court Street Plant
Syracuse, NY 13201

Prof. K.C. Yeh
University of Illinois
Dept. of Electric Engineering
Urbana, IL 61801

Dr. Warren Brown
Sandia Lab
ORG 314
Albuquerque, NM 87115

Dr. C.H. Liu
60 Electrical Engineering
Building
University of Illinois
Urbana, IL 61801

Dr. S. Ossakow
Plasma Dynamics, Code 7750
U.S. Naval Research Lab
Washington, D.C. 20390

Dr. Phil McClure
U. of Texas at Dallas
Richardson, TX 75080

Prof. H.G. Booker
Dept. of Applied Physics
U. of Calif. at San Diego
La Jolla, CA 92037

Prof. Michael Kelley
Dept. of Elect. Engineering
Cornell University
Ithaca, NY 14850

Prof. W.B. Hanson
U. of Texas at Dallas
Richardson, TX 75080


END
FILMED
6-83
DTIC